2012

Characterization and Modeling of Pneumatic Multi-Material Micro-Extrusion

Tejas Bendarkar

ROCHESTER INSTITUTE OF TECHNOLOGY

Characterization and Modeling of Pneumatic Multi-Material Micro-Extrusion

A Thesis submitted in partial fulfillment of the

Requirements for the degree of

Masters of Science in Industrial Engineering

In the

Department of Industrial & Systems Engineering

Kate Gleason College of Engineering

By

Tejas Bendarkar

M.S., Industrial Engineering, Rochester Institute of Technology, 2012

KATE GLEASON COLLEGE OF ENGINEERING

ROCHESTER INSTITUTE OF TECHNOLOGY

ROCHESTER, NEW YORK

CERTIFICATE OF APPROVAL

August 24th 2012

M.S. DEGREE THESIS

The M.S. Degree Thesis of Tejas Bendarkar

has been examined and approved by the

thesis committee as satisfactory for the

thesis requirement for the

Masters of Science degree.

Approved by:

Dr. Denis Cormier, Thesis Advisor

Dr. Marcos Esterman, Committee Member

Dr. Andres Carrano, Committee Member

ABSTRACT

Functionally Graded Materials (FGMs) are characterized by a continuous variation in the composition of parent materials through the work piece volume. This gradual change in material composition is aimed at improving mechanical, thermal and/or electrical properties of the material. FGMs are being increasingly used in a variety of applications including aerospace, biomedical and nuclear.

FGMs have been produced using additive manufacturing processes such as laser engineered net shaping (LENS) and 3D printing. A relatively new process category called direct write (DW) printing has evolved over the past decade. DW techniques such as multi-material micro-extrusion are capable of producing FGMs. To fully utilize the capabilities of multi-material micro-extrusion, experimentation and modeling is needed to determine the factors that significantly affect the mass flow rate and proportion of each nanoink being dispensed. The objectives of this study were to develop a parametric model for multi-material pneumatic micro-extrusion and to develop equations to determine the parameter values to achieve the desired ink proportions during ink deposition.

Experiments were conducted using red, blue and yellow acrylic inks that were printed using a commercially available three material pneumatic micro-extruder from nScrypt. Preliminary experiments determined that air pressure and valve needle position were significant parameters affecting the mass flow rate of the inks. A 2^6 experiment was then designed and carried out. Parametric equations thus developed provided relationships between the parameter values and the proportions of inks dispensed. The equations were validated by solving them using an AMPL linear program. For a given desired proportion of inks to be dispensed, the AMPL program suggests process parameter values needed to produce the desired multi-material output.

ACKNOWLEDGEMENTS

I would like to thank my thesis advisor, Dr. Denis Cormier, for the opportunity to work in an exciting research area, and his support through the course of the study. I would also like to thank my thesis committee members, Dr. Marcos Esterman and Dr. Andres Carrano for their guidance through the length of this work.

I am also grateful for the help and support of fellow students Anuj Datar and Sundaresan Balasubramanian with my lab work and experimentation. I would also like to thank my family for their love and continual support throughout my education.

TABLE OF CONTENTS

LIST OF FIGURES

LIST OF TABLES

LIST OF EQUATIONS

CHAPTER 1: INTRODUCTION

1.1 FUNCTIONALLY GRADED MATERIALS

A functionally graded material (FGM) is a multi-material composite manufactured by varying the composition and structure over a specified volume. As the composition of the constituent materials continuously varies as a function of position to yield a predetermined microstructure, FGMs can be tailored for different applications to suit the desired properties (Miyamoto, Kaysser, Rabin, Kawasaki, & Ford, 1999). The ability of FGMs to have tailored composition helps to provide unique solutions to complex engineering problems. Early research into FGMs involved two-material thermal barrier coatings for use in aerospace and nuclear energy applications. In thermal barrier coatings, the composition of the FGM is gradually transitioned from a metal based substrate to a ceramic based coating. By eliminating abrupt transitions in material composition in FGMs, there is improved resistance to delamination along the interfaces. In laminated composite materials, there is a tendency for the material to crack at the interfaces; this problem is mitigated in FGMs by the gradual change in the composition of materials.

FGMs are often used in high temperature environments such as thermal barrier coatings, aerospace, and nuclear applications. However, recent studies in FGMs also focus on applications in biomedical engineering and surface coating applications that increase the wear resistance and electrical properties (Domack & Baughman, 2005).

1.2 APPLICATIONS OF FUNCTIONALLY GRADED MATERIALS (FGMS)

As discussed above, functionally graded materials are primarily used in high temperature applications such as thermal barrier coatings, aerospace and nuclear engineering,

biomedical applications and surface coating applications. Some of the interesting applications of functionally graded materials are discussed below.

1.2.1 AEROSPACE ENGINEERING

Homogeneous materials such as metals become increasingly prone to oxidation, creep, and low strength at elevated temperatures, limiting their use in high temperature applications. Ceramics developed to overcome these problems often have a dissimilar coefficient of thermal expansion (CTE) than the metal substrate (Erdogan, 1995). FGMs have been used in thermal barrier coatings in which the amount of ceramic is varied through the coating thickness, thus giving rise to a non-homogeneous composition providing the desired thermal properties (Kawasaki & Watanabe, 2002).

Conventional thermal shielding in an aircraft is done using high temperature resistant laminated structures such as ceramic tiles used on NASA's space shuttle. Since these structures are laminated to the aircraft substructure, the difference in CTE between the ceramic tiles and the substructure can lead to problems at elevated temperatures. The CTE mismatch can cause stress concentrations between the ceramic tiles and the aircraft substructure that supports them, resulting in cracking and de-bonding as shown in Figure 1. To avoid cracking and delamination at the boundary of two surfaces due to high shear stress, FGMs are being used to replace conventional thermal shielding in aircraft structures. (Cooley, 2005)

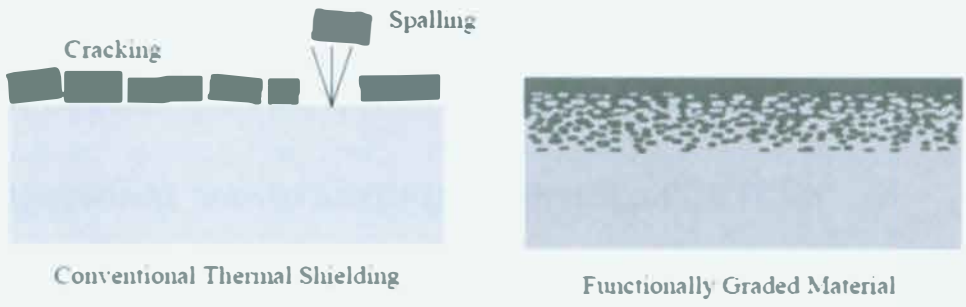

Figure 1: Advantages of FGM in aircraft structures (Cooley, 2005)

In addition to thermal barrier coatings, functionally graded materials have applications for load bearing structures and surface coatings to reduce wear and corrosion. In a drive to improve the efficiency and to reduce the operating cost and weight of aerospace structures, FGMs are being incorporated in the shells of aircrafts and space shuttles (Sankar, 2001) to reduce the effects of vibration, wear, corrosion, and uneven heat transfer (Göransson, 2008).

1.2.2 BIOMEDICAL APPLICATIONS

FGMs are being used in artificial bone scaffolds since they can be manufactured to have a dense and strong external structure to a soft and porous internal structure. Research on developing new and better biomaterials for medical applications has been reviewed in a study by Pompe et al. (Pompe et al., 2003) An important aspect of this research is to develop biologically inspired materials. In the development of replacement teeth and bones, hydroxylapatite (HA, Ca_5 $(PO_4)_3OH$) is the main mineral constituent which shows excellent biocompatibility with bone, skin and muscle tissues. HA exhibits minimal cytoxic effects and allows the bone to re-grow on the FGM due to its porosity. However, it has relatively poor mechanical properties and hence cannot be used for heavy load bearing applications. To overcome this problem, Chenglin et al. (Chenglin, Jingchuan, Zhongda, & Shidong, 1999) developed a functionally graded HA-Ti material through a powder metallurgy process. The gradual distribution of components in a FGM can eliminate the abrupt macroscopic interface, such as that in a direct joint between two materials.

Considering the large number of applications for FGM's, numerous processing routes have been investigated. These methods are reviewed in the following section.

1.3 TRADITIONAL MANUFACTURING METHODS FOR FGMS

The traditional methods for manufacturing FGMs typically consist of producing a spatially graded powder material which is then consolidated using an appropriate technique. Due to

increasing amounts of research in the field of functionally graded materials, a variety of manufacturing processes have been developed. These processes range from powder metallurgy techniques to additive manufacturing methods.

1.3.1 ULTRASONIC CONSOLIDATION

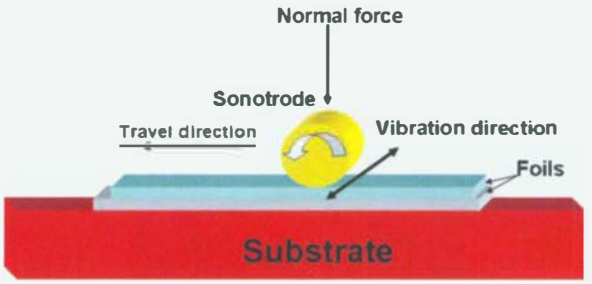

Figure 2: Ultrasonic consolidation process (S. Kumar, 2010)

Kumar used ultrasonic consolidation to manufacture graded composition materials using aluminum (Al), copper (Cu) and stainless steel foils. (S. Kumar, 2010) These foils were joined together using an ultrasonic consolidation process developed by Solidica Inc., USA. Ultrasonic consolidation is similar to ultrasonic welding in which high frequency ultrasonic vibrations are locally applied to metal foils drawn from a stock coil held at high pressure. This creates a solid state weld between the foil and the substrates as seen in Figure 2. A welding head called a sonorode is vibrated as the foil is fed into the machine. The substrate is placed on a heated platen which is held at a temperature below the melting temperature of the foil and substrate material(s). The ultrasonic vibrating head normal to the direction of travel is made to contact the metal foils. This force helps the two foils to bond without melting.

1.3.2 LASER ENGINEERED NET SHAPING (LENS)

The Laser Engineered Net Shape process (LENS) used by Domack et al. (Domack & Baughman, 2005) is capable of producing FGMs. LENS is a powder deposition process in which one or more metal powders are blown into a moving melt pool created as a laser beam is scanned over a work piece. This adds material to the surface of the work piece and is therefore

classified as a laser additive manufacturing process. To enable deposition of FGMs, multiple nozzles are used to deposit powder in the desired proportions as shown in Figure 3. This process was developed at Sandia National Laboratories and was mainly used for thin walled parts. The LENS process can be modified to produce thick walled parts as demonstrated by Zhao et al. (Zhao et al., 2009) using nickel (Ni), cu and tin (Sn).

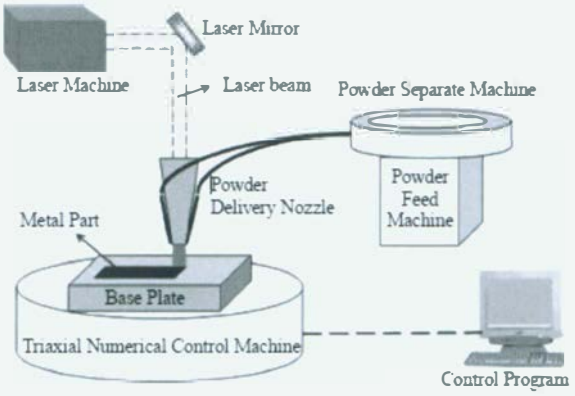

Figure 3: Schematic diagram of LENS process (Zhao et al., 2009)

1.3.3 POWDER METALLURGY APPROACHES

Similar to traditional powder metallurgy processes, manufacturing of FGMs using powder metallurgy involves powder production, powder forming, pressing, and sintering. The required composition for the FGM can be obtained by varying the powder particles in the pre-formed mixture. Zua et al. (Zhu, Lai, Yin, Jeon, & Lee, 2001) developed a powder metal FGM part consisting of partially stabilized zirconia (PSZ) and nickel chromium alloy (Ni-Cr). PSZ was blended together using a ball mill to make fine powder that was then mixed with the NiCr alloy. The advantage thus obtained by using powder metallurgy for FGM manufacturing is that the composition of the final part can be easily controlled by varying the pre-formed powder composition (Chenglin et al., 1999). Figure 4 shows a schematic diagram of the powder metallurgy process. Accurate quantities of materials are weighed and mixed using a V-mill. Depending on the configuration of FGM desired, the powders are stacked as shown in Figure 4

(c). After the powders are stacked, they are sintered to create the required FGM. (Yoshimi & Hisashi, 2011)

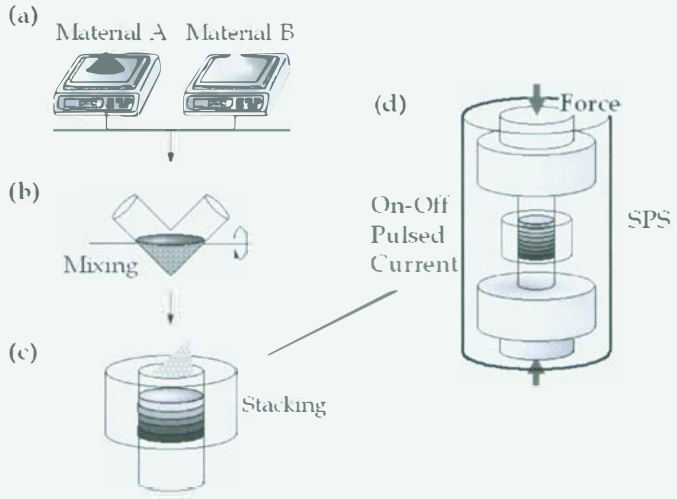

Figure 4: Schematic diagram of powder metallurgy process (Yoshimi & Hisashi, 2011)

1.3.4 SELECTIVE LASER SINTERING (SLS)

The selective laser sintering process begins with design the required geometry on CAD software, such as Solidworks. Figure 5 shows a schematic diagram of the selective laser sintering process. The CAD file is converted into the STL format, where it is sliced layer by layer and fed into the SLS machine. A high power laser beam is selectively scanned over the powder bed, thus fusing the material in its path. The scanning path is generated from the STL file. After each cross-section is fused, the powder bed is lowered, a new layer of powder is applied on the top of the previous one, and the process continues. The SLS process was developed by DTM Corporation which has since been acquired by 3D Systems (Sanjay Kumar, 2003). Chung et al. (Chung & Das, 2006) demonstrated the application of SLS to produce FGMs. The material deposition process was modified to produce a graded powder composition between successive layers as well as within each layer to create a functionally graded part. A Sinterstation 2000 was used with glass-filled Nylon-11.

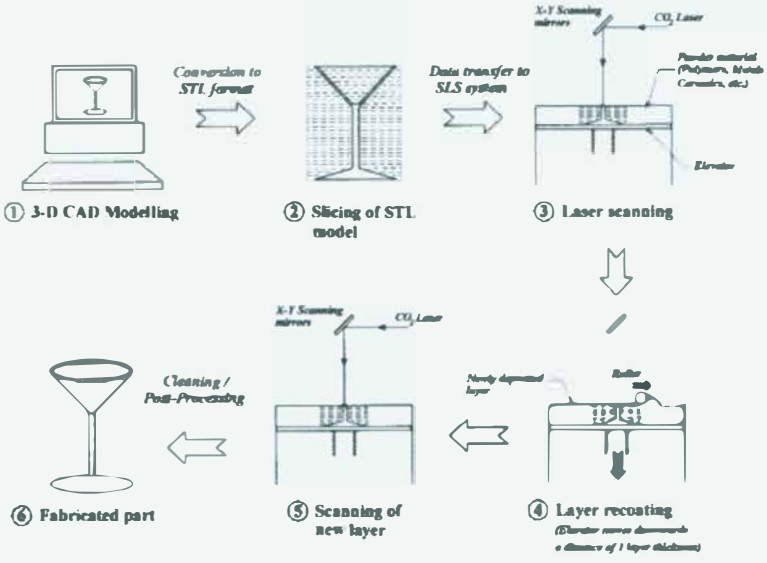

Figure 5: Schematic diagram of selective laser sintering (Tan et al., 2003)

Apart from traditional methods of manufacturing, a new class of rapid prototyping technique called direct-write has been developed to print FGMs on to a given substrate. Chapter 2 reviews the most commonly used direct write processes and gives an overview of the basic process parameters. Chapter 3 explains the research methodologies for ink preparation, preliminary experiments and final experiments to measure the proportion of inks dispensed. The results of the experiments are discussed in Chapter 4. Chapter 5 concludes the study with the summary of results and a discussion of future work.

CHAPTER 2: LITERATURE REVIEW

Apart from traditional methods of manufacturing, novel direct-write (DW) methods for the fabrication of FGMs on planar and non-planar surfaces are gaining popularity. The complexity of the structure determines the DW technology and the fabrication materials required. DW processes differ from conventional rapid prototyping processes in a few ways. First, the width of material deposited on the substrate ranges from hundreds of nanometers to millimeters. Second, the substrate used in the process is an integral part of final geometry (Hon, Li, & Hutchings, 2008). The following section describes some of the direct-write processes found in the literature.

2.1 DIRECT-WRITE METHOD OF MANUFACTURE

Important DW technologies include nozzle dispensing methods, transfer methods and laser systems for modifying or depositing materials. An extensive range of materials may be used as a substrate for direct writing.

2.1.1 INK JET BASED DW

Over the last few decades, inkjet printing has become a commonplace method for printing on paper, cans, packaging, etc. In recent years, however, functional multilayer parts have been manufactured directly using inkjet printers with nanoinks (Hon et al., 2008). The materials that can be inkjet-printed range from sol-gels to metals (Calvert, 2001). After inkjet deposition, the nanoink typically solidifies due to solvent evaporation, the application of thermal energy, or solvent reaction. After printing the required part, sintering may be carried out on as needed basis. The nozzle orifice diameter, ink viscosity and surface tension are critical parameters for this process (Gibson, Rosen, & Stucker, 2009).

Several applications for ink jet printing have been reported in the literature. Ink jet printing of yttria-stabilized zirconia was carried out by Young et al. (Young et al., 2008) to develop anode based solid oxide fuel cells. The manufacture of sintered ceramic molds for metal casting processes can be carried out by printing binders on the required ceramic powder. After a layer of binder is printed, a new layer of ceramic is rolled on the top. The shape thus is sintered to obtain the final geometry. (Calvert, 2001)

Inkjet printing of low temperature and viscosity liquid metal has be demonstrated for printed circuit board applications. This forms the basis of printed electronics. Uniform bead lengths of 100 μm were obtained. (Calvert, 2001)

The two commonly used inkjet printing techniques are continuous printing and drop on demand. Figure 6 (a) shows the basic idea behind the continuous printing process. In continuous printing, a continuous stream of ink droplets is generated from the nozzle. A piezoelectric crystal located within the nozzle creates vibrations that break up the continuous bead into individual droplets. A range of 64,000 to 165,000 droplets per second can be achieved. The droplets are then electrostatically deflected to the correct write areas of the substrate. The droplets which do not get electrostatically deflected continue to a collection chamber for reuse (Hon et al., 2008).

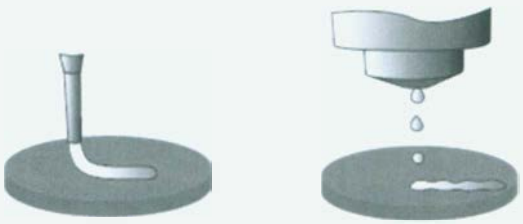

Figure 6: (a) Continuous inkjet printing (b) Drop on demand printing

Figure 6 (b) shows drop on demand printing. In drop on demand printing, a single ink drop is generated using a trigger pulse only when required. The trigger signal is provided by a

controller to a thermally heated nozzle which forms a small bubble of vapor. After the bubble bursts, the ink is ejected and the nozzle is filled with ink from the reservoir. Piezoelectric or acoustic effects are also widely used in drop on demand processes (Hon et al., 2008). The drop on demand process can be scaled up using multiple nozzles. All the inkjet processes described above print a single ink per dispensing head. If multiple inks are required to be printed simultaneously, multiple dispensing heads are used.

2.1.2 ENERGY BEAM BASED DIRECT WRITE TECHNOLOGIES

In energy beam based DW technologies, energy beams in the form of laser or ion beams are used to create the desired features. Depending on the energy source used, the processes are further classified into:

a. Laser chemical vapor deposition (LCVD)
b. Laser enhanced electroless plating
c. Focused ion beam direct writing
d. Focused ion beam direct writing

These processes have been described in greater detail in following sections.

Laser chemical vapor deposition (LCVD)

Laser direct write technologies use a pulsed laser to transfer material from a source to a substrate which is close to or in contact with it. It thus achieves non lithographic processing on the substrate (Piqué 2010). A variety of materials including metals, ceramics, semi-conductors, polymers, composites and biomaterials have been successfully used (Hon et al., 2008). Figure 7 shows a schematic diagram of the laser assisted chemical vapor deposition process to produce carbon nanotubes (Alexandrescu et al., 2003). It consists of a flow reactor in which a silicon wafer substrate is mounted. The flow reactor is driven by a mechanically actuated pump.

Mixtures of reactant gases are allowed into the reaction cell close to the silicon wafer. A laser beam is impinged at the surface to create a reaction at gas/substrate interface.

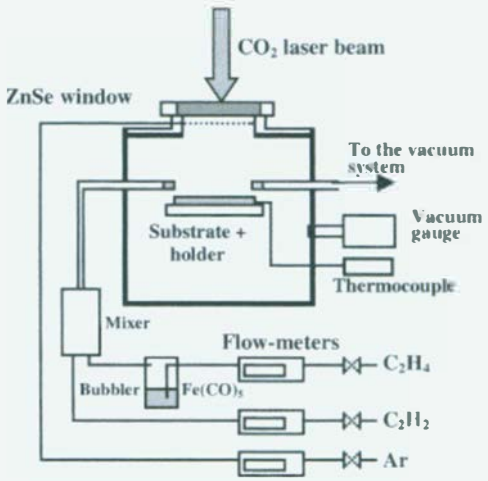

Figure 7: Schematic diagram of laser chemical vapor deposition (Alexandrescu et al., 2003)

Laser enhanced electroless plating

Von Gutfeld et al. (Von Gutfeld & Romankiw, 1982) developed a technique for depositing and etching metals immersed in aqueous solutions containing metallic ions required for deposition using a focused laser beam. Due to the large local increase in current density where the laser is focused on the cathode, the plating or etching rate is considerably higher in this region. The localized high temperature causes decomposition of the liquid and deposition of a metallic layer on the substrate (Puippe, Acosta, & Von Gutfeld, 1981). The researchers carried out experiments in Pyrex glass cells with vertical electrodes. The anode, made up of a copper plate, included a small hole which was used to a direct laser beam onto a thin film cathode. The researchers found that the enhancement of the reaction rate was primarily due to the increase in the temperature at the metal solution interface.

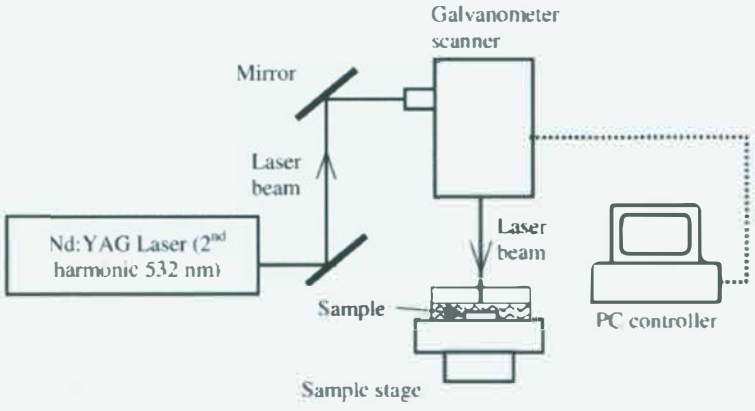

Figure 8: Schematic setup for laser electroless plating (Wang, Zheng, & Lim, 2002)

The experimental setup used by Wang et al. (Wang et al., 2002) for metal deposition on to the sample substrate to create printed electronics is shown in Figure 8. The laser beam used was directed to the galvanometer using multiple reflecting mirrors. The galvanometer scanner is computer controlled and used to position the laser beam on the substrate immersed in the electrolyte. Different copper patterns can be directly written on the substrate by movement of the laser.

Focused ion beam direct writing (FIB)

In a focused ion beam (FIB) direct writing process, liquid gallium is placed in contact with a tungsten needle and is then heated. After application of an electric field, a beam of gallium ions are emitted. The emitted ions are further accelerated and focused into nanometer range spot sizes using electrostatic lenses. The collision of ions on the substrate causes the following mechanisms as outlined by Hon et al. (Hon et al., 2008): sputtering of neutral and ionized substrate atoms, electron emission, displacement of atoms in the solid, and emission of photons. The use of FIB as a direct write technology is somewhat similar to the laser chemical vapor deposition (CVD) process. Instead of a laser beam, a FIB source is scanned over the substrate in the presence of a gaseous precursor (C.-S. Kim, Ahn, & Jang, 2012). The main advantage of using FIB as an energy source is the better resolution obtained when compared with laser CVD. Figure 9 shows a schematic diagram of focused ion beam used in deposition.

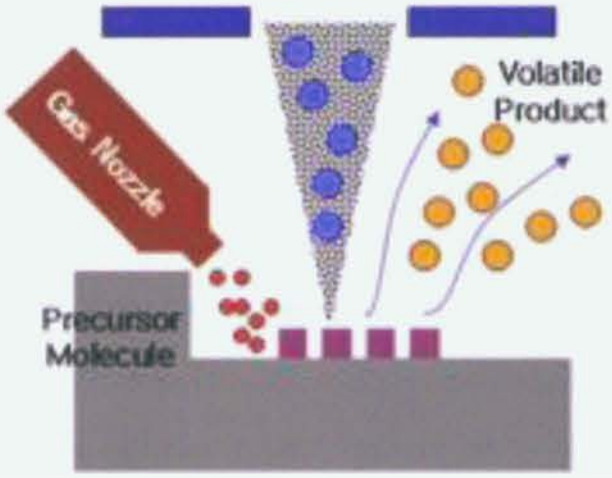

Figure 9: Focused ion beam used in material deposition (C.-S. Kim et al., 2012)

2.1.3 FLOW BASED DIRECT WRITING

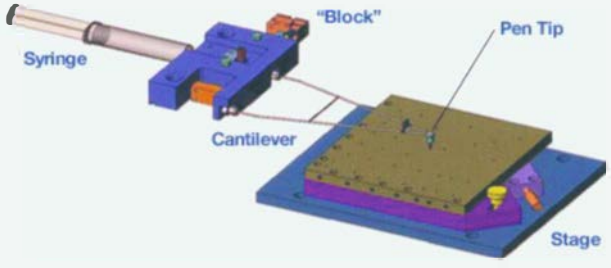

Figure 10: Working of Micropen DW technology (B. Li, Clark, & Church, 2007)

In flow based direct writing processes, a liquid ink is typically extruded from a syringe onto a substrate using either air pressure or a mechanical plunger. The amount of material dispensed is dependent on the pressure applied to the syringe and the amount of time it is applied (Li B., 2007). The micro-pump technology developed by nScrypt uses accurately controllable air pressure, timing, valve opening and dispensing height. The pump is provided with a suction function which removes residual material at the tip of the nozzle, which increases the dispensing precision.

OhmCraft Inc. developed a similar micro-capillary technology under the trade name of Micropen. The working of a micropen is shown in Figure 10. Material to be deposited is

prepared in slurry form and is injected into the writing head via a pneumatic ram. The pressure generated due to positive displacement of the ram forces the material out of the dispensing tip. The tip traverses the surface of the substrate in the prescribed path without direct contact.

The selection of materials for direct write processes mainly depends on the application of the final product. To manufacture of high strength gears for medical devices micro-dispensing, Kim et al. (W. J. Kim & Sa, 2006) developed a micro-extrusion machine to extrude equal channel angular pressed magnesium prepared from Mg-AZ31 alloy. The result demonstrated that high strength micro-gears could be obtained through grain refinement and texture control. The rheology of inks plays an important role to determine the micro-dispensing abilities. Smay et al. (Smay, 2002) developed a V-shaped test structure using a robotic deposition nozzle to determine that there is a strong relationship between rheology of ink prepared and the pH value. During the study, plumbum zirconate titanate (PZT) was pre-adsorbed as a dispersant and suspended into an aqueous solution of 0.5% wt. of methocel F4M in deionized water.

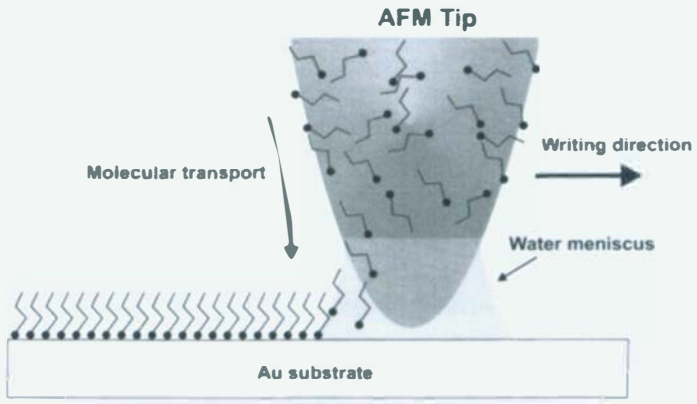

Figure 11: Schematic representation of DPN showing molecular transport between AFM tip and Au Substrate (Ginger, Zhang, & Mirkin, 2004)

2.1.4 TIP BASED DIRECT WRITING

Tip based direct writing processes are further classified into dip pen nanolithography and nano fountain pen direct writing. Dip pen lithography is a direct-write scanning probe tip based technique developed by Nano Ink Inc. (Ginger et al., 2004). Figure 11 shows a schematic diagram of dip pen nanolithography showing molecular transportation between tip and substrate. An ink coated Atomic Force Multiplier (AFM) tip is used to pattern chemicals directly to the substrate using capillary action. It is a constructive lithographic tool used to produce a variety features in metals and semiconductors with controlled properties (Ginger et al., 2004) The process can be used to print a wide variety of inks, organic molecules, DNA, nano particles, metal ions, etc. However, DPN does not have a continuous ink feeding system (Salaita, Wang, & Mirkin, 2007).

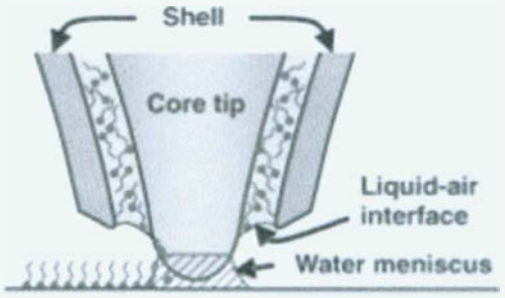

Figure 12: Working of Nanofountain pen (Ginger et al., 2004)

Micropipettes, often known as NanoFountain Pens (NFP), have been developed to overcome this disadvantage in DPN. Figure 12 shows the working of nanofountain pens. The pen contains a volcano shaped tip used to transport molecular ink stored in the reservoir to gold (Au) substrate. The ink is transported using built-in micro-channels via capillary action. The ink at the tip causes a surface of liquid air interface, and when the tip is made to contact the substrate, the ink is deposited on the substrate. Proteins, active enzymes, DNA and polymers can be deposited using NFP (K. H. Kim, Moldovan, & Espinosa, 2005).

2.2 MULTI – MATERIAL PRINTING SYSTEMS

The recent advances in material printing have enabled the fabrication of parts with localized composition control to achieve a uniform transition between two or more materials. The applications of functionally graded material discussed earlier in this chapter have opened the door for wide spread research in multi material printing systems. Some commonly used multi-material printing systems are as follows

a. Aerosol Jet Printing
b. Multi-nozzle ink jet printing
c. Robocasting process
d. Multi-material micro-dispensing

2.2.1 AEROSOL JET PRINTING

Figure 13: (a) Schematic diagram of Aerosol Jet Process (www.optomec.com); (b) Optomec equipment used in the lab

The Aerosol Jet printing technique is capable of multi-material deposition. Figure 13 (a) shows a schematic diagram to explain the working of the aerosol jet printing process. The first step in Aerosol Jet direct write printing is the generation of aerosol mist from the source material to produce droplets in the order of a couple of microns. The generation of aerosol mist takes place in the atomizing chamber from where the aerosol mist gets densified in the virtual

impactor. From the virtual impactor, the dense gas is transported to the deposition head where a sheath gas is introduced to focus the tiny droplets into a thin collimated beam. This beam exits the deposition head and impinges on the substrate due to its momentum to create the required pattern. Figure 13 (b) shows the Optomec equipment used at RIT. The Aerosol Jet printing process is widely used to fabricate printed electronics on the order of 10 to 100 μm wide. A single nozzle system is capable of writing at speeds up to 200 mm/s and volumetric deposition rates of 0.25 mm^3/s. Pál et al. have reported the printing of Cu-Ni alloy based ink using the Aerosol Jet process to fabricate printed microstructures (Pál et al., 2012). Su et al. manufactured cadmium selenium (Cd-Se) polycrystalline thin films for solar cells (Su & Choy, 2000). The optical band gap values obtained for such printed cells were between 1.63-1.65 eV, hence they are suitable for photovoltaic applications.

2.2.2 MULTI NOZZLE PRINTING

Li et al. (L. Li et al., 2009) developed a multi nozzle inkjet drop on demand system for the fabrication of 3D tissue scaffolds. The system can be used to dispense multiple materials from individual nozzles at the commanded positions. There are two parts to the system. The software control system receives the solid model from any 3D design software. The hardware control system consists of the motor control, the synchronizer, and the pressure control as shown in Figure 14.

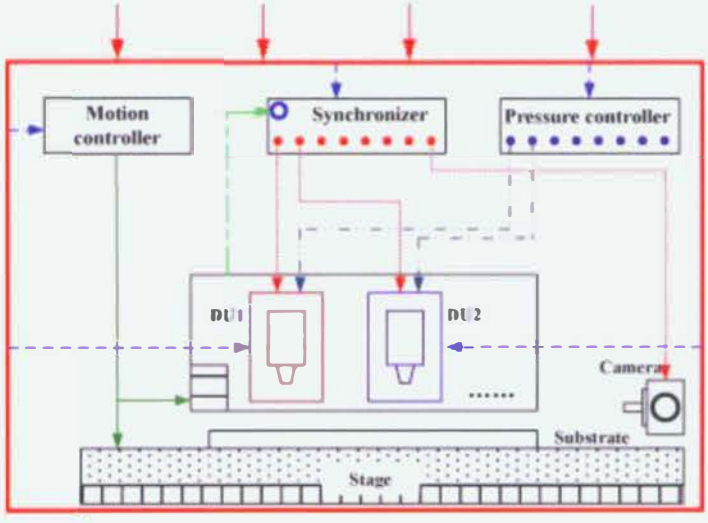

Figure 14: Hardware control in multi nozzle printing system (L. Li et al., 2009)

The motor control receives commands from the software to drive the motion stages. After the commanded position has been reached, the synchronizer is activated to control the multiple dispensing units (DU) as required. The DUs dispense the required micro-droplets onto the substrate. The pressure controller is used to control the back pressure by providing a positive and/or negative pressure on the dispensing nozzles.

2.2.3 ROBOCASTING PROCESS

Robocasting is a direct write process developed by Sandia National Laboratories around the same time as nScrypt developed its micro-extrusion process. The two approaches are conceptually very similar. Figure 15 shows a schematic diagram of a single material robocasting machine. Syringes filled with concentrated ceramic slurries to be dispensed are loaded in the syringe and dispensed through a ceramic nozzle using robotically controlled deposition. The slurry is prepared by mixing the required ceramic powder, water and chemical additives (Cesarano, King, & Denham, 1998 Dec 01).

Miranda et al. (Miranda, Saiz, Gryn, & Tomsia, 2006) have used robocasting with β-tricalcium phosphate (TCP, $Ca_3(PO_4)_2$) to develop porous bone scaffold structures to repair damaged bones. A syringe was filled with paste prepared by mixing powder with water and

chemical additives. The paste was deposited through conical nozzles to produce the required 3D scaffold geometry. The scaffold geometry is based on the bone or tissue that is to be replaced.

Li et al. (Li B., 2007) determined that the porosity and spatial organization of cells following implantation of the scaffold has a pronounced impact on the performance of the scaffold. Some common disadvantages of prosthetic implants such as loosening of the implant and mechanical failure were overcome through optimization of the implant geometry.

Smith et al. (Smay, 2002) developed clinically viable prostheses by printing a 3D polycaprolactone (PCL) scaffold on top of a modified titanium construct. The resultant implant thus allows for direct anchoring to the bone. This overcomes common difficulties of pain and infection at the point of contact.

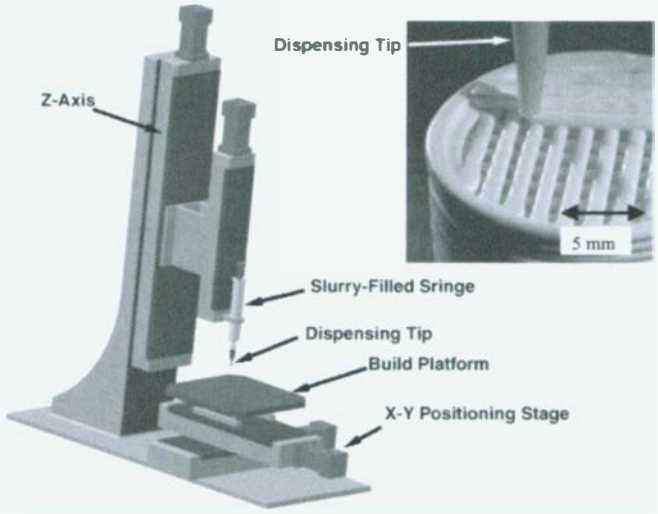

Figure 15: Schematic of a three-axis single material robocasting machine (Stuecker, Cesarano Iii, & Hirschfeld, 2003)

2.2.4 MULTI-MATERIAL MICRODISPENSING

nScrypt, formed in October 2002, is based on Sciperio's Micro-dispense Direct-Write (MDDW) technology. MDDW was developed through the DARPA (Defense Advanced Research

Projects Agency) MICE program (Mesoscopic Integrated Conformal Electronics). The nScrypt system uses a computer aided design (CAD) model to build 2D or 3D models. The substrate platen can precisely move in the X-Y plane at any desired velocity within a specified range. The dispensing nozzle can move in the Z direction. By incorporating a precision Z stage with a height sensor, printing on non-planar surfaces is possible. The valve design of dispensing tool allows ink to be sucked back at the end of a path segment in order to provide precise control over printed features. The conical shape of the nozzle tip makes dispensing of liquids up to 1,000,000 cP possible. The software allows users to precisely control air pressure, timing, needle position and dispensing height of the nozzle. Li et al. (B. Li et al., 2007) studied the manufacturing of miniaturized devices and assemblies using the nScrypt smart pump. The researchers also printed scaffolds for tissue and organ replacing using the smart pump. Polycaprolactone (PCL) dissolved in acetic acid at 40% concentration was used for the experiments (Li B., 2007). Xu et al (Dongjiang Xu, 2009) developed a method to manufacture die stacks and vertical interconnection for integrated circuits. A single material smart pump was used for the process. The resulting die stacks can be mounted directly on the integrated circuit boards.

Figure 16 (a) shows a Smart Pump developed by nScrypt with arrows indicating the dispensing tip and pressurized inlet valve. The Smart Pump is capable of printing a single ink at a time. Figure 16 (b) shows the three ink multi-mixer developed by nScrypt used in the study. The basic working of the multi-mixer is similar to the smart pump, but it can dispense three inks at a time.

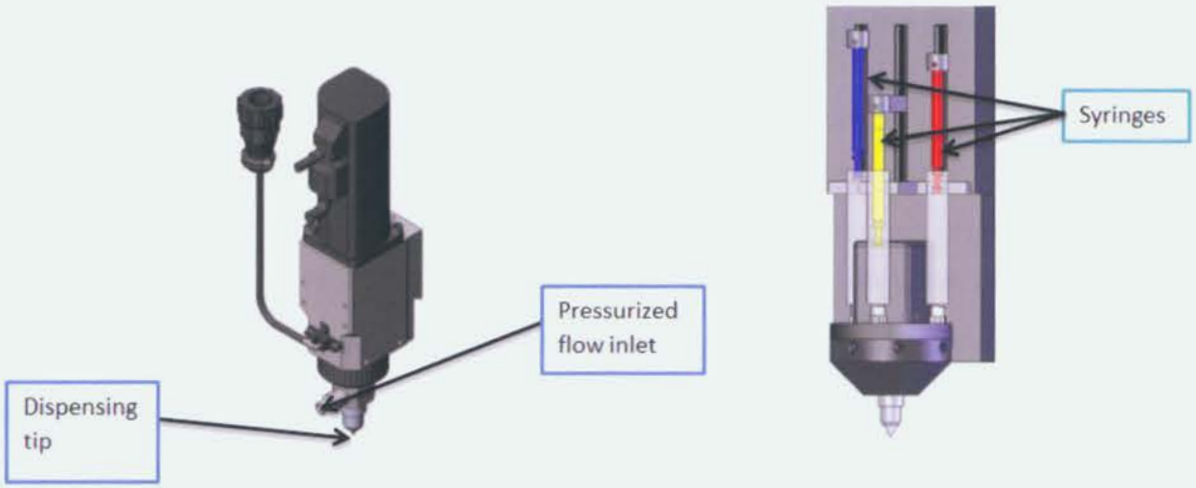

Figure 16: (a) Smart Pump; (b) Multi-mixer by nScrypt systems (www.nscrypt.com)

Instead of using multiple nozzles to print multi-materials, nScrypt developed a micro mixer pump capable of mixing three materials on the fly in any proportion before they are dispensed. A sample color pattern produced by nScrypt using a multi-material mixer is shown in Figure 17 (a). This demonstration shows mixing of the three color inks printed without any boundary between different colors. Multi nozzle printing does not produce true functionally graded components since mixing of homogenous inks with different porosity does not occur in multi nozzle deposition process.

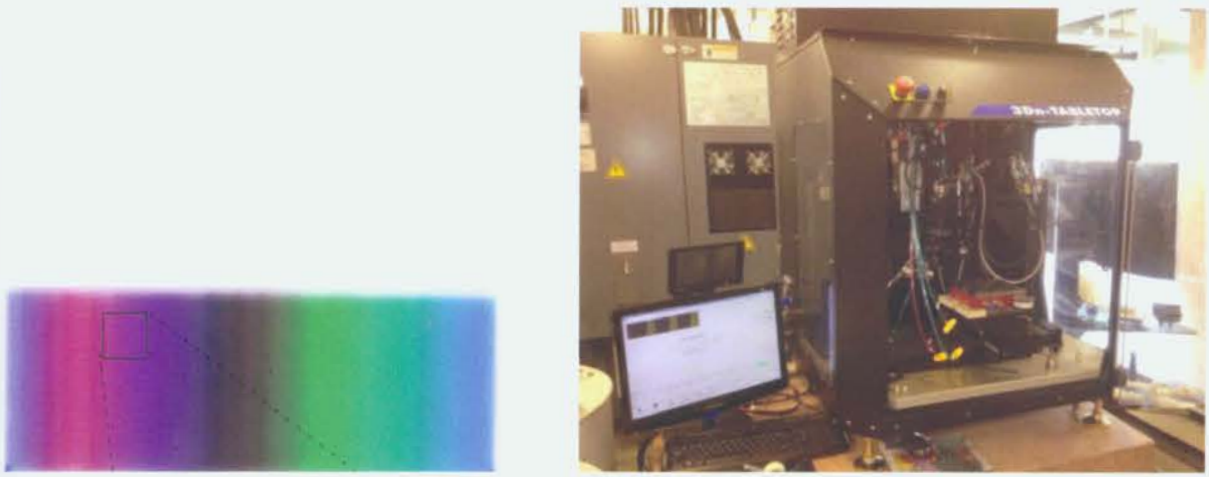

Figure 17: (a) Patterns produced using on-the-fly printing. (b) Tabletop multi-mixer used (www.nscrypt.com)

Figure 17 (b) shows an nScrypt table top printer at RIT with the three component active mixing system, commonly known as a micro-mixer. Some advantages of multi-material micro-extrusion

include the ability to work with highly viscous inks, the ability to mix inks on the fly before deposition, and the ability to print inks on non-planar surfaces.

2.3 STATEMENT OF NEED

As seen from Section 2.2, there has been a lot of research done pertaining to single material micro-extrusion of thick pastes using direct-write processes via a variety of actuation methods (e.g. pneumatic, positive displacement, etc.). However, there has been little research on multi-material pneumatic micro-dispensing. Specifically, there is little understanding of how the many process parameters influence the relative proportions and flow rates of multi-material dispensing systems. The aim of this research is to get a better understanding of which process parameters have the most significant influence, and the extent to which they influence process output.

CHAPTER 3: RESEARCH METHODOLOGY

This chapter discusses the research methodology carried out in the study. Section 3.1 deals with procedure to prepare inks for each experimental run combination. Section 3.2 explains the working of a commercially available nScrypt multi-mixer used in the study and the different parameters affecting it. Further sections provide the design for preliminary flow rate experiments and the final composition experiment.

3.1 INK PREPARATION

Red, blue and yellow acrylic inks from Golden Artist Colors Inc. were used for experimental purposes. To keep the viscosity of inks similar for the duration of the experiments, 5 grams of ink with 0.5 ml of ethylene glycol was mixed together using a THINKY ARM 310 mixer spinning at 2000 rpm for 5 minutes. Ink mixing is facilitated using centrifugal forces of over 400G which enables simultaneous mixing, dispersion and de-aeration to create a thoroughly mixed ink. All inks used in this research were prepared using this method unless specified otherwise. Ethylene glycol is a low vapor pressure solvent that was used to increase the drying time of the inks and to reduce the viscosity. Viscosity is one of the most important factors affecting the mass flow rate of an ink for particular settings (Gibson et al., 2009). To minimize the potential of ink viscosity changing over time (e.g. solvent drying), new set of inks were freshly prepared for each set of experiments.

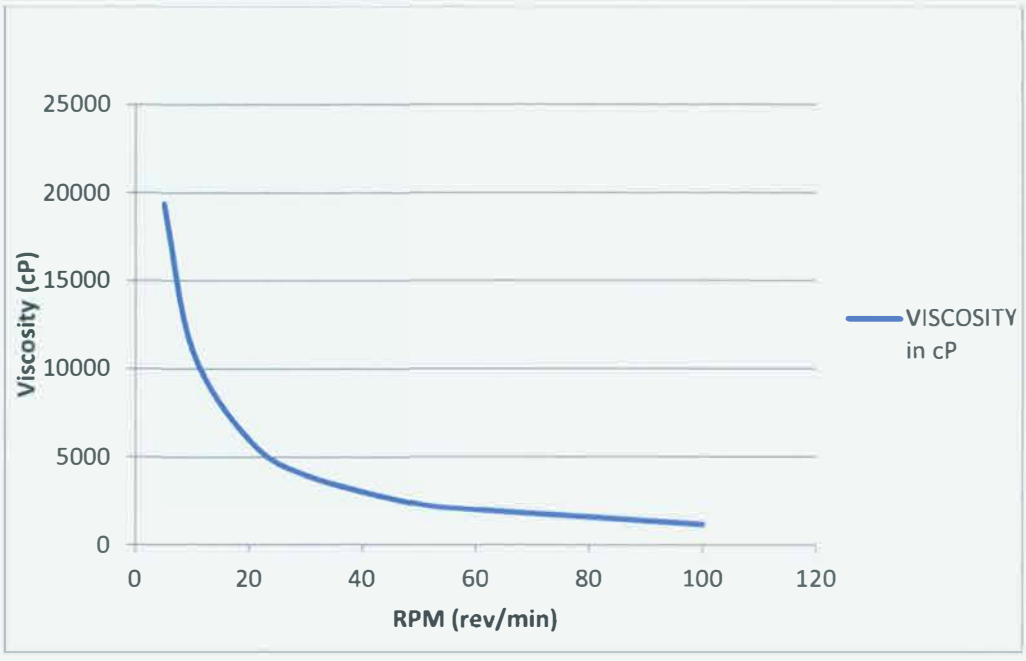

Figure 18: Ink viscosity (cP) v/s spindle RPM (rev/min)

Ink viscosities were measured using a Brookfield viscometer with an S63 spindle. The spindle was rotated at various speeds to produce different shear rates, and the measured viscosity was recorded. Figure 18 shows the relationship between spindle speed (rev/min) and the viscosity of the ink. From Figure 18, we conclude that these acrylic inks display nonlinear decaying behavior and hence they are non-Newtonian shear thinning inks. For a direct writing process, it is preferable to use a shear thinning ink than a shear thickening ink, as the viscosity of the ink will be reduced as the ink flows through the nozzle tip (B. Li et al., 2007).

3.2 NSCRYPT PROCESS DESCRIPTION

The nScrypt table top micro dispensing system used in this research employs a three axis motion control system where the work table moves in the X and Y axis directions, and the micro-dispensing head moves in the Z-axis direction. For this research, the three material micro-mixer was used. The ink to be extruded in each of the three dispensing valves is loaded into a 3cc plastic syringe barrel. The three syringe barrels are then attached to their respective valve bodies using a threaded 10-32-to-luer fitting adapter. A regulated air pressure source is

connected to the syringe. The air pressure provides force that pushes the ink/paste from the syringe barrel into the valve body. When the valve needle is opened, the ink flows through the body into the ceramic nozzle. The process is akin to turning a water faucet on or off in that the position of the valve stem at a given pressure will determine the liquid flow rate. The user can insert ceramic nozzle tips having diameters that typically range from 25 to 150 μm. The diameter of the ceramic nozzle may influence flow rates as well as the width of the printed track. The valve needle position and the magnitude of air pressure can be adjusted on the fly using the control software provided with the system. The nScrypt multi-mixer used in this work is shown in Figure 19 and Figure 20. The movement of the table in the X and Y axes is controlled by tool path software provided with the system.

The flow rate of each ink is independently controlled via three servo motors that raise or lower the valve rods. The movement of the valve rods dictates the amount of ink that can flow through the opening. Air pressure is directly applied to each syringe barrel attached to extruder locations A, B and C as shown. The movement of the needle in a downward position opens up the valves. Together with the applied air pressure, this causes ink to flow into the mixing chamber. A rotating stainless steel fluted rod in the mixing chamber is used to mix the three materials. The mixed ink flows through the attached ceramic nozzle. The size of the nozzle determines the cross sectional area of the ink dispensed.

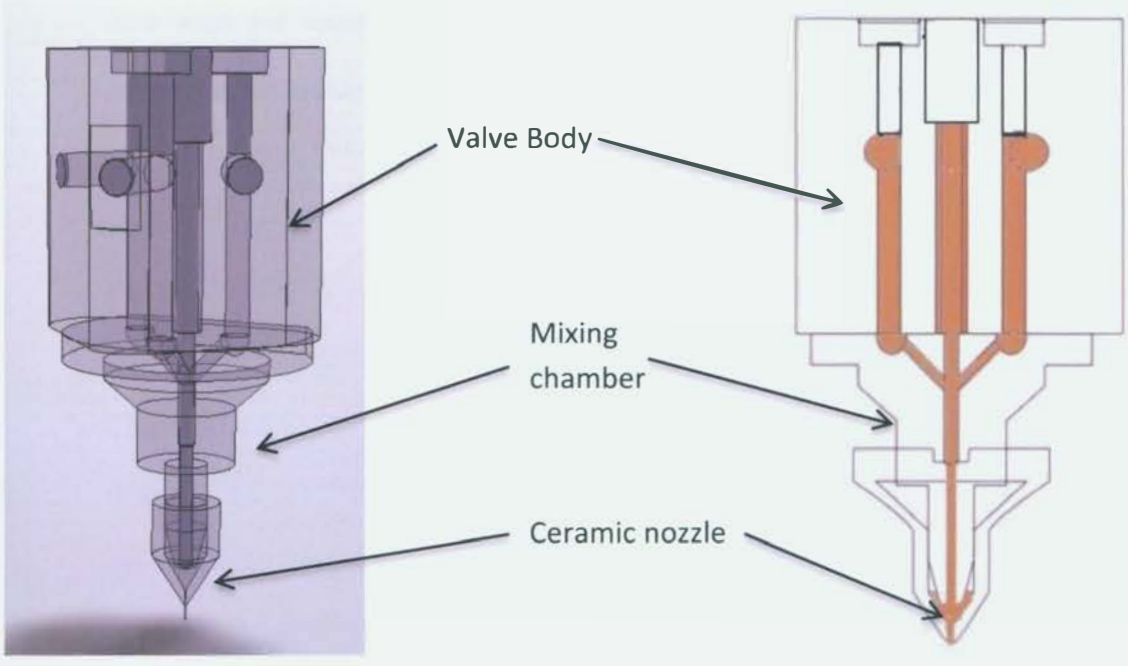

Figure 19: (A) nScrypt multi-mixer; (B) multi-mixer cross sectional area

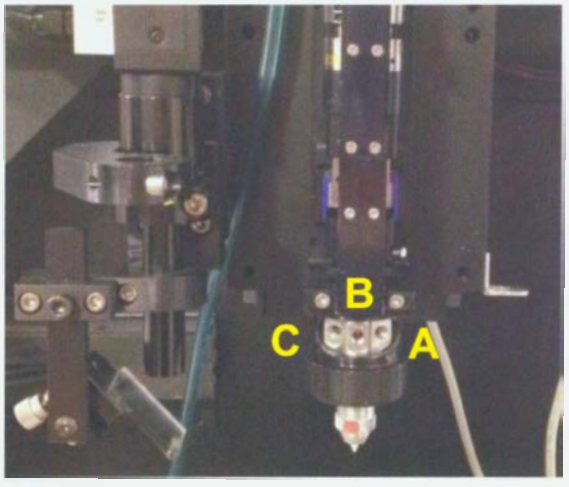

Figure 20: Z Stage micro-mixer used with table top printer

The major elements that a user can control with this process that may affect the mass flow rate are summarized as follows:

1. Extruder location – The multi-material micro-extruder has three separate extruder locations as seen in Figure 20. As there is a left (A), center (B) and right (C) valve, it is possible that the extruder locations could influence the output response of a given ink.

The extruder locations (A, B and C) are therefore considered to be one of the experimental factors.

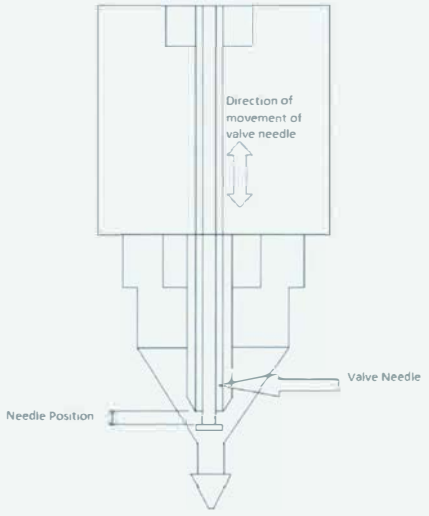

Figure 21: Schematic diagram explaining needle position

2. Needle position (mm) – Each of the three ink valves has a separate needle that is opened or closed to allow or disallow the flow of ink. The farther the needle is extended in the mixing chamber, the more ink is permitted to flow. This is true up to the point where the needle doesn't restrict the flow at all. The position of each of the three valve needles is measured in millimeters. Figure 21 shows a schematic diagram explaining the needle position. For simplicity, only one needle is shown in the diagram.
3. Air pressure (psi) – Each of the three ink valves has its own independently controllable air pressure regulator. As the air pressure applied to the ink increases, the flow rate should also increase provided the needle valve is open and the pressure is sufficiently large to cause the flow of ink. The nScrypt toolpath file does not directly use air pressures. Rather, an analog voltage value is specified for the regulator that produces a corresponding air pressure. For instance, a value of 0.9 volts produces an air pressure of approximately 18 psi. Hence air pressure for each of the three extruders is the third factor to be considered.

4. Ink – For this research, three acrylic pigment inks (yellow, blue and red) were used to facilitate data analysis through image processing. In order to assess whether or not the color of ink has any influence on output, ink color was also considered as a factor.
5. Motion delay (msec) – The nScrypt toolpath program has a built in feature which delays the movement of the nozzle at the start point. This delay gives ink time to flow from the tip to the substrate before movement begins.
6. Standoff distance (mm) – The distance between the tip of nozzle and the substrate is measured in millimeters. This affects the bead cross section and uniformity of the print. If the distance is smaller than the bead diameter, then the resulting bead is compressed and spreads laterally as it exits the nozzle. If it is excessively large, then surface tension may cause the extruded bead to break up into discontinuous segments. Figure 22 shows a diagram explaining the standoff distance.

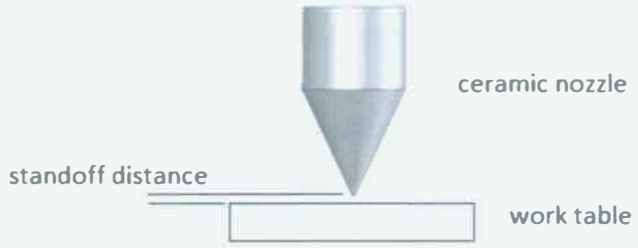

Figure 22: Schematic diagram showing standoff distance

7. Feed rate (mm/sec) – This is the travel speed at which the nozzle moves during printing. It influences the flow of material per unit length. Feed rate and standoff distance together influence width and continuity of the print. If the travel speed exceeds the velocity at which the extrudate exits the nozzle, the extrudate is placed in tension and will either stretch or break up into discontinuous segments. If the feed rate is slower than the extrudate velocity, then the extrudate will bunch up and spread laterally. Figure 23 (a) & (b) show the effects of feed rate on the ink bead quality.

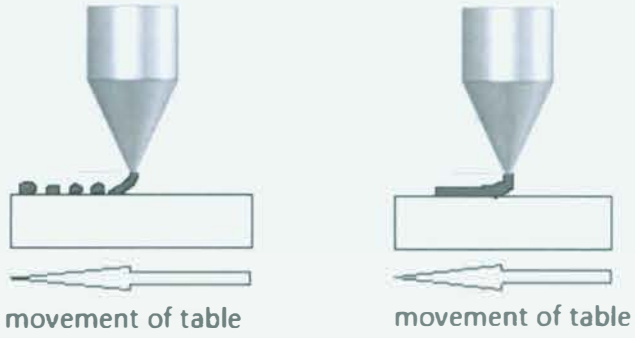

Figure 23: (a) Showing high feed rate. (b) Acceptable feed rate

8. Nozzle diameter (μm) – This is the inner diameter of the nozzle opening. Nozzles are available in standard sizes of 12.5 μm, 25 μm, 50 μm, 75 μm, 100 μm, and 125 μm. Nozzle size affects the ink shear rate, the flow rate of the ink, and the width/thickness of the extruded bead.
9. Ink viscosity (cP) – The property of the ink that affects the ink flow in the system. It has been hypothesized that for a given set of process parameters, inks with lower viscosity will have a higher flow rate than inks with higher viscosity.

To determine the factors that affect mass flow rate of inks and their proportions, a flow rate experiment was carried out with design as shown in Table 1. The response measured was mass flow rate of inks. A final composition experiment was carried out using factors which were found to affect the mass flow rate of inks. The response for the final composition experiment was the proportion of each of the three inks dispensed. Using a general linear model, equations are developed to provide the relationship between process parameters and the ink proportions. The model thus developed was validated using a linear program and two experimental validation runs.

Table 1: Flow rate experimental design

Factors	Number of Levels
Extruder Location	3
Needle Position	2
Ink	3
Air Pressure	2

Factors:	4	Replicates:	3
Base runs:	36	Total runs:	108
Base blocks:	1	Total blocks:	1

Number of levels: 3, 2, 2, 3

3.3 FLOW RATE EXPERIMENTS

The aim of the flow rate experiments was to determine the effects of different color inks and the needle position on the mass flow rate of the inks. Section 3.2 discusses the primary factors that can affect the flow rate. The experiment was used to identify the most significant factors for further study in the composition experiments. During initial lab work with the nScrypt multi-mixer, it was determined that the valve opening/closing speed, motion delay, standoff distance, and feed rate have little effect on the ink flow rates. These factors appear to affect the line width and thickness. However line width and thickness are not the focus of this work. This result was also observed by Khatri-Chhetri (Khatri-Chhetri, 2011). For all the experiments, the nozzle diameter used was 125 μm. Ink particle size can affect the mass flow rate of the inks through the system. Since this study only considers acrylic inks from Golden Artist Colors, Inc, this was not considered in the flow rate experiment. To reduce potential variability in ink viscosity, freshly prepared ink was used for each trial. Ink color (Yellow, Blue, Red) was considered as one of the factors. Hence for the preliminary flow rate experiments, the following factors were considered:

1. Extruder Location (Levels A, B or C) as shown in Figure 20
2. Needle position (for each extruder location A, B, and C)
3. Air pressure (for each extruder location A, B, and C)
4. Ink color – Yellow, Blue and Red

The inks were prepared as per the procedure previously described. A series of experiments as detailed in Table 1 and Table 2 were conducted. For each run configuration, the ink was allowed to flow into an aluminum weigh cup for 30 seconds. The mass of each weigh cup was measured before and after each trial run, and the difference between the values gave the mass of ink dispensed in 30 seconds (i.e. the mass flow rate in mg/min). To reduce variation due to air bubbles trapped in the system, a three replicate design was considered for flow rate experiments.

Table 2: Factor levels for flow rate experiments

	Parameters				
Levels	Needle Position (mm)	Air Pressure		Ink Color	Extruder Location
		Regulator Voltage (Volts)	psi		
1	1.48	0.90	18	Yellow	A
2	-	-	-	Blue	B
3	1.60	1.50	30	Red	C

A trial and error experiment was first carried out to determine the operating limits of parameters under consideration. Observation from these experiments indicated that that the acrylic inks started to flow at a needle position of 1.48 mm. below this value, there was no ink flow observed for any value of air pressure. The maximum needle position ("wide open" valve position) was determined by the motor travel limit of the valve needle. In this case, the limit was 1.78 mm. However, a maximum needle position value of 1.60 mm was used due to the fact that beyond this position, any increase in the needle position value did not affect the mass flow rate of the inks. At a needle position of 1.48 mm, the minimum air pressure required to induce the flow of ink was 18 psi. Air pressures above 30 psi at the wide open needle position of 1.60 mm produced unacceptably large and unstable flow rates.

It was observed that frequent changing of needle position and air pressure during experimentation resulted in air bubbles being introduced in the system. The effects of air bubbles present in the system are not fully understood, but they were seen to induce excessive

variation in mass flow rate. Randomization of runs is ideally carried out to spread the effect of uncontrollable variations among residuals. If the runs are not randomized the effects of uncontrollable factors may affect the response variable. For this experiment, solvent evaporation for the ink is considered as an uncontrollable factor. As the runs are not randomized, solvent evaporation may add errors into the mass flow rate. However, due to excessive variations in mass flow rate from air bubbles produced by changing needle positions, the experimental runs were not randomized in this case and the parameters were not continuously varied. The resultant experimental design is a general full factorial design without randomization. The ideal design in this case would be a full factorial design with complete randomization. Such a design would spread out the effect of solvent evaporation over the entire experimental runs. The experimental table for the flow rate experiment thus generated in Minitab is shown in Table 3. To improve the interpretability of the residual graphs obtained from Minitab, a square root transformation of the mass flow rate data was carried out.

Table 3: Experimental table for flow rate experiment

Run Order	Extruder Location	Pressure	Needle Opening Position	Ink	Flow Rate (gm/sec)		Run Order	Extruder Location	Pressure	Needle Opening Position	Ink	Flow Rate (gm/sec)
1	1	1	1	1	0.0030		20	2	2	1	1	0.0060
37	1	1	1	2	0.0023		56	2	2	1	2	0.0057
73	1	1	1	3	0.0027		92	2	2	1	3	0.0060
4	1	1	2	1	0.0043		23	2	2	2	1	0.0333
40	1	1	2	2	0.0047		59	2	2	2	2	0.0400
76	1	1	2	3	0.0047		95	2	2	2	3	0.0367
7	1	2	1	1	0.0057		26	3	1	1	1	0.0027
43	1	2	1	2	0.0060		62	3	1	1	2	0.0020
79	1	2	1	3	0.0057		98	3	1	1	3	0.0023
10	1	2	2	1	0.0367		29	3	1	2	1	0.0043
46	1	2	2	2	0.0367		65	3	1	2	2	0.0047
82	1	2	2	3	0.0400		101	3	1	2	3	0.0043
13	2	1	1	1	0.0023		32	3	2	1	1	0.0060
49	2	1	1	2	0.0030		68	3	2	1	2	0.0060
85	2	1	1	3	0.0027		104	3	2	1	3	0.0057
16	2	1	2	1	0.0043		35	3	2	2	1	0.0367
52	2	1	2	2	0.0050		71	3	2	2	2	0.0367
88	2	1	2	3	0.0047		107	3	2	2	3	0.0400
19	2	2	1	1	0.0060		3	1	1	1	1	0.0027
55	2	2	1	2	0.0060		39	1	1	1	2	0.0027
91	2	2	1	3	0.0057		75	1	1	1	3	0.0023
22	2	2	2	1	0.0333		6	1	1	2	1	0.0047
58	2	2	2	2	0.0400		42	1	1	2	2	0.0050
94	2	2	2	3	0.0367		78	1	1	2	3	0.0050
25	3	1	1	1	0.0027		9	1	2	1	1	0.0060
61	3	1	1	2	0.0020		45	1	2	1	2	0.0060
97	3	1	1	3	0.0027		81	1	2	1	3	0.0060
28	3	1	2	1	0.0047		12	1	2	2	1	0.0400
64	3	1	2	2	0.0047		48	1	2	2	2	0.0333
100	3	1	2	3	0.0050		84	1	2	2	3	0.0367
31	3	2	1	1	0.0060		15	2	1	1	1	0.0023
67	3	2	1	2	0.0060		51	2	1	1	2	0.0023
103	3	2	1	3	0.0057		87	2	1	1	3	0.0023
34	3	2	2	1	0.0400		18	2	1	2	1	0.0047
70	3	2	2	2	0.0367		54	2	1	2	2	0.0047
106	3	2	2	3	0.0400		90	2	1	2	3	0.0043
2	1	1	1	1	0.0027		21	2	2	1	1	0.0060
38	1	1	1	2	0.0023		57	2	2	1	2	0.0060
74	1	1	1	3	0.0023		93	2	2	1	3	0.0057
5	1	1	2	1	0.0047		24	2	2	2	1	0.0367
41	1	1	2	2	0.0053		60	2	2	2	2	0.0367
77	1	1	2	3	0.0050		96	2	2	2	3	0.0367
8	1	2	1	1	0.0060		27	3	1	1	1	0.0020
44	1	2	1	2	0.0060		63	3	1	1	2	0.0023
80	1	2	1	3	0.0057		99	3	1	1	3	0.0023
11	1	2	2	1	0.0333		30	3	1	2	1	0.0047
47	1	2	2	2	0.0367		66	3	1	2	2	0.0047
83	1	2	2	3	0.0400		102	3	1	2	3	0.0050
14	2	1	1	1	0.0030		33	3	2	1	1	0.0057
50	2	1	1	2	0.0023		69	3	2	1	2	0.0053
86	2	1	1	3	0.0023		105	3	2	1	3	0.0060
17	2	1	2	1	0.0043		36	3	2	2	1	0.0400
53	2	1	2	2	0.0047		72	3	2	2	2	0.0400
89	2	1	2	3	0.0043		108	3	2	2	3	0.0367

3.4 COMPOSITION EXPERIMENTS

From the flow rate experiments, it was observed that needle position and air pressure values were significant factors that affect the mass flow rate of the ink. The flow rate experiments were carried out to identify mass flow rates of individual inks at different extruder location in the nScrypt multi-material deposition system. The end goal of the study is to develop a model to predict factor values for the proportions of inks dispensed. The proportions of extruded inks calculated can be considered a measure of their individual mass flow rate when extruding the inks simultaneously. Hence, significant factors from the first experiment were considered significant in the composition experiments carried out. The response used for the composition experiment was the proportion of yellow, red and blue inks in the printed lines.

One observation during the flow rate experiments was the fact that differences in factor values have an effect on the mass flow rate between three inks in the multi-mixer. As a result, an experiment was devised to highlight the effects of differences in pressure and needle position for inks at extruder location A, B and C on their proportions. Since air pressure and needle position for individual extruder locations are independently controlled, the air pressure and needle position for extruder location A were set at values shown in Table 4. The pressure and needle position values for extruder location B and C were set to values that are a delta (pressure/needle position differential) greater or less than that of extruder location A. The flow rate experiments executed previously study the flow of a single ink through the multi-mixer deposition system. In the composition experiments, three inks were extruded simultaneously for the given experimental conditions to measure proportion dispensed. Since the needle position and air pressure for each extruder location are independently controlled; the factors for composition experiments are as shown below.

- Pa and Oa are the air pressure and needle position values for extruder location A.

- Pb and Ob are the air pressure and needle position values for extruder location B.
- Pc and Oc are the air pressure and needle position values for extruder location C.

Table 4: Factor levels for composition experiments

Variable	Low	High
Pa	1.1	1.3
ΔPb	-0.2	0.2
ΔPc	-0.2	0.2
Oa	1.52	1.56
ΔOb	-0.04	0.04
ΔOc	-0.04	0.04

3.4.1 COMPOSITION EXPERIMENTAL SETUP

A 2^6 experiment was designed with factor levels as shown in Table 4 to determine the effects of parameter values on the relative proportions of the three color inks dispensed. For each experiment, ink was prepared as discussed in Section 3.1. Ten lines were printed on photographic inkjet paper and allowed to air dry for 30 minutes. Ten lines were printed to allow the system to reach a steady state before readings were taken. For each trial, a cross section of the dried ink sample was taken. Three cross-sections for each trial were analyzed using Hirox digital microscope model KH-770 under magnification 150X to ensure the output was reasonably consistent. For each trial, ImageJ software was used to measure the area of each color using the procedure described below in Section 3.4.2. It is important to highlight that no mixing was used when the inks were dispensed. This was done to facilitate the measurement of ink colors through image analysis. The relative proportions of each color are the response for composition experiments.

As discussed in Section 3.3, the minimum air pressure was 0.9V and maximum air pressure considered was 1.5V. Similarly, the minimum/maximum needle positions considered were 1.48mm and 1.6mm. In order to consider factor values spanning entire operating range, values of Pa, Oa and delta were fixed as shown in Table 4.

As discussed in Section 4.1.1, the extruder location A, B and C did not affect the mass flow rate of the ink. Hence ink extruder location was not considered for this experiment. To provide a standard set of procedures for all the final experimental runs, yellow ink was loaded in extruder location A, blue ink was loaded in extruder location B, and red ink was loaded in extruder location C.

The variables considered are summarized as follows:

- **Pa** is the air pressure (volts) applied at extruder location A
- **Pb** is the differential in the applied air pressure (volts) between extruder location A and extruder location B
- **Pc** is the differential in the applied air pressure (volts) between extruder location A and extruder location C
- **Oa** is the needle position (mm) at extruder location A
- **Ob** is the differential in the needle position (mm) between extruder locations A and B
- **Oc** is the differential in the needle position (mm) between extruder locations A and C

The variables Pa, Pb, Pc and Oa, Ob, Oc are independently controlled variables. The response measured is the proportional cross sectional area of three inks dispensed.

As discussed previously in Section 3.3, frequent change in air pressure and needle opening values resulted in air bubbles being introduced in the system. Air bubbles thus introduced will cause undue variation in the mass flow rate of inks and thus in the proportions of inks dispensed. To avoid presence of air bubbles, randomization of runs was not carried out. The resultant design is a 2^6 full factorial design with no randomization. The detailed experimental table obtained from Minitab is provided in Table 5.

Table 5: Design of composition experiments generated from Minitab

Run Order	Parameters						Response		
	Pa (Volts)	Pb (Volts)	Pc (Volts)	Oa (mm)	Ob (mm)	Oc (mm)	Proportion of Ink Yellow	Proportion of Ink Blue	Proportion of Ink Red
1	1.10	0.90	0.90	1.52	1.48	1.48	0.68	0.15	0.17
2	1.30	1.10	1.10	1.52	1.48	1.48	0.63	0.2	0.17
3	1.10	1.30	0.90	1.52	1.48	1.48	0.48	0.33	0.19
4	1.30	1.50	1.10	1.52	1.48	1.48	0.51	0.32	0.17
5	1.10	0.90	1.10	1.52	1.48	1.48	0.64	0.11	0.25
6	1.30	1.10	1.50	1.52	1.48	1.48	0.61	0.18	0.21
7	1.10	1.30	1.30	1.52	1.48	1.48	0.58	0.22	0.2
8	1.30	1.50	1.50	1.52	1.48	1.48	0.4	0.29	0.31
9	1.10	0.90	0.90	1.56	1.52	1.52	0.41	0.28	0.31
10	1.30	1.10	1.10	1.56	1.52	1.52	0.65	0.14	0.21
11	1.10	1.30	0.90	1.56	1.52	1.52	0.29	0.58	0.13
12	1.30	1.50	1.10	1.56	1.52	1.52	0.33	0.52	0.15
13	1.10	0.90	1.30	1.56	1.52	1.52	0.62	0.17	0.21
14	1.30	1.10	1.50	1.56	1.52	1.52	0.64	0.14	0.22
15	1.10	1.30	1.30	1.56	1.52	1.52	0.5	0.27	0.23
16	1.30	1.50	1.50	1.56	1.52	1.52	0.45	0.27	0.28
17	1.10	0.90	0.90	1.52	1.56	1.48	0.14	0.51	0.35
18	1.30	1.10	1.10	1.52	1.56	1.48	0.37	0.41	0.22
19	1.10	1.30	0.90	1.52	1.56	1.48	0.19	0.69	0.12
20	1.30	1.50	1.10	1.52	1.56	1.48	0.49	0.32	0.19
21	1.10	0.90	1.30	1.52	1.56	1.48	0.26	0.41	0.33
22	1.30	1.10	1.50	1.52	1.56	1.48	0.32	0.41	0.27
23	1.10	1.30	1.30	1.52	1.56	1.48	0.31	0.52	0.17
24	1.30	1.50	1.50	1.52	1.56	1.48	0.13	0.55	0.32
25	1.10	0.90	0.90	1.56	1.60	1.52	0.42	0.34	0.24
26	1.30	1.10	1.10	1.56	1.60	1.52	0.51	0.31	0.19
27	1.10	1.30	0.90	1.56	1.60	1.52	0.25	0.63	0.12
28	1.30	1.50	1.10	1.56	1.60	1.52	0.38	0.51	0.11
29	1.10	0.90	1.30	1.56	1.60	1.52	0.34	0.4	0.36
30	1.30	1.10	1.50	1.56	1.60	1.52	0.25	0.35	0.4
31	1.10	1.30	1.30	1.56	1.60	1.52	0.37	0.49	0.14
32	1.30	1.50	1.50	1.56	1.60	1.52	0.28	0.61	0.11
33	1.10	0.90	0.90	1.52	1.48	1.56	0.43	0.22	0.35
34	1.30	1.10	1.10	1.52	1.48	1.56	0.37	0.18	0.45
35	1.10	1.30	0.90	1.52	1.48	1.56	0.48	0.29	0.23
36	1.30	1.50	1.10	1.52	1.48	1.56	0.42	0.21	0.37
37	1.10	0.90	1.30	1.52	1.48	1.56	0.28	0.11	0.61
38	1.30	1.10	1.50	1.52	1.48	1.56	0.32	0.16	0.52
39	1.10	1.30	1.30	1.52	1.48	1.56	0.28	0.14	0.58
40	1.30	1.50	1.50	1.52	1.48	1.56	0.24	0.24	0.52
41	1.10	0.90	0.90	1.56	1.52	1.60	0.55	0.14	0.31

Run Order	Parameters						Response		
	Pa (Volts)	Pb (Volts)	Pc (Volts)	Oa (mm)	Ob (mm)	Oc (mm)	Proportion of Ink Yellow	Proportion of Ink Blue	Proportion of Ink Red
42	1.30	1.10	1.10	1.56	1.52	1.60	0.47	0.19	0.34
43	1.10	1.30	0.90	1.56	1.52	1.60	0.37	0.23	0.4
44	1.30	1.50	1.10	1.56	1.52	1.60	0.51	0.19	0.3
45	1.10	0.90	1.30	1.56	1.52	1.60	0.25	0.17	0.58
46	1.30	1.10	1.50	1.56	1.52	1.60	0.2	0.18	0.62
47	1.10	1.30	1.30	1.56	1.52	1.60	0.23	0.24	0.53
48	1.30	1.50	1.50	1.56	1.52	1.60	0.31	0.21	0.48
49	1.10	0.90	0.90	1.52	1.56	1.56	0.34	0.3	0.36
50	1.30	1.10	1.10	1.52	1.56	1.56	0.45	0.31	0.24
51	1.10	1.30	0.90	1.52	1.56	1.56	0.45	0.34	0.21
52	1.30	1.50	1.10	1.52	1.56	1.56	0.25	0.53	0.22
53	1.10	0.90	1.30	1.52	1.56	1.56	0.33	0.26	0.41
54	1.30	1.10	1.50	1.52	1.56	1.56	0.14	0.28	0.58
55	1.10	1.30	1.30	1.52	1.56	1.56	0.13	0.45	0.42
56	1.30	1.50	1.50	1.52	1.56	1.56	0.2	0.42	0.38
57	1.10	0.90	0.90	1.56	1.60	1.60	0.47	0.3	0.23
58	1.30	1.10	1.10	1.56	1.60	1.60	0.22	0.37	0.41
59	1.10	1.30	0.90	1.56	1.60	1.60	0.28	0.61	0.11
60	1.30	1.50	1.10	1.56	1.60	1.60	0.16	0.64	0.2
61	1.10	0.90	1.30	1.56	1.60	1.60	0.28	0.13	0.59
62	1.30	1.10	1.30	1.56	1.60	1.60	0.27	0.19	0.54
63	1.10	1.30	1.30	1.56	1.60	1.60	0.19	0.39	0.42
64	1.30	1.50	1.50	1.56	1.60	1.60	0.27	0.35	0.38

3.4.2 PROCEDURE FOR MEASURING CROSS SECTIONAL AREAS

To measure the cross-sectional area of each ink, the printed samples were held against the glass plate with half of the sample extending beyond the surface. Using the glass plate edge as support the samples were cut with scissors at a halfway point in the length of the printed line. Care was taken to ensure that the samples were cut perpendicular to the print direction. The cut sample was attached to a glass plate using clear tape and clips. The glass plate was mounted at a right angle to the surface plate of the Hirox microscope with help of small clay pieces as shown in Figure 24. The cross-sectional area of each ink sample was viewed at 150X magnification. Three cross-sectional micrographs for each experimental run were visually

analyzed under the microscope to ensure the ink proportions were reasonably constant (Figure 25). A single micrograph was then analyzed using ImageJ (Figure 26).

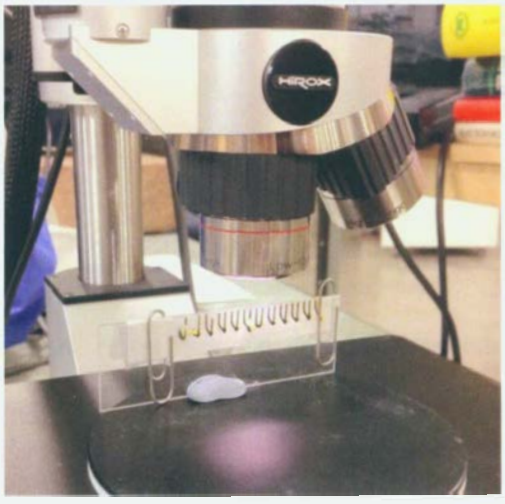

Figure 24: Method to view cross-section of sample under microscope

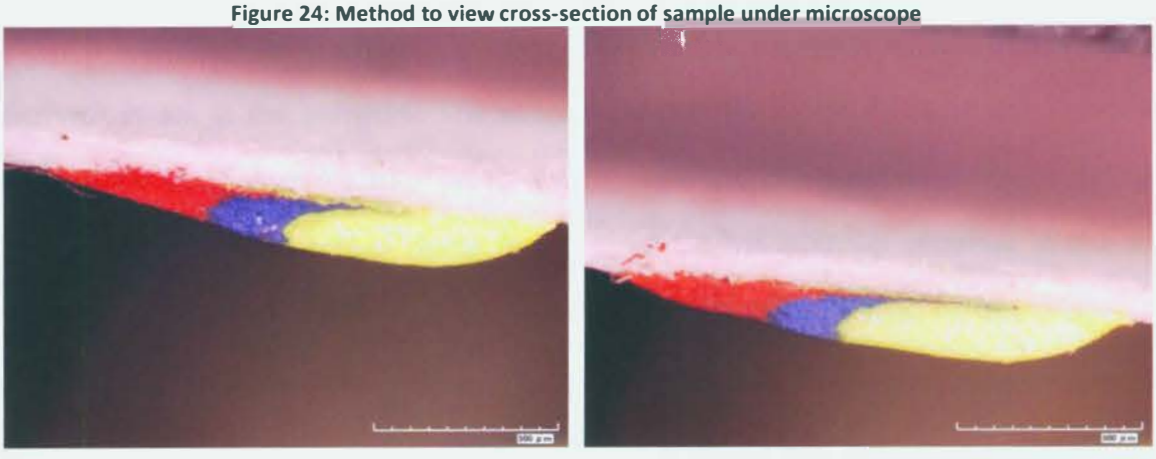

Figure 25: Comparison of multiple samples for consistency

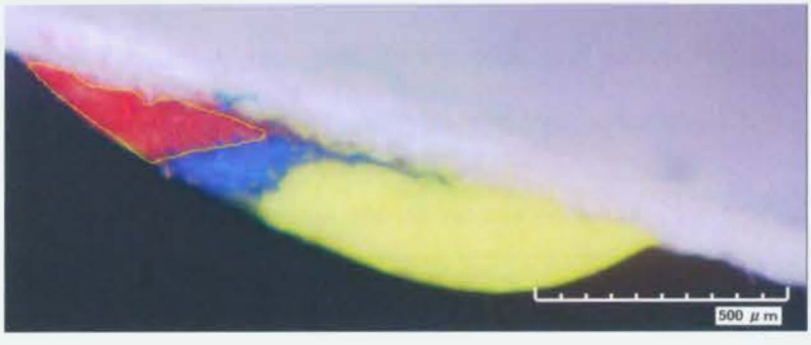

Figure 26: Sample microscopic image indicating cross sectional area for run 13

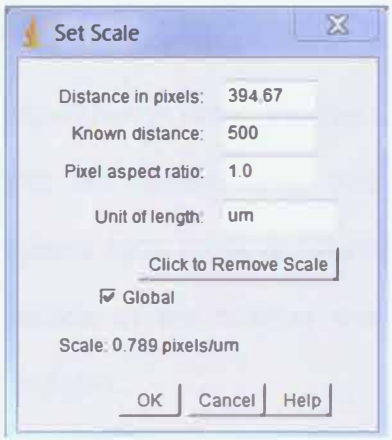

Figure 27: Set scale example for ImageJ

ImageJ is a java based open source image processing program designed and developed by the National Institutes of Health (Collins, July 2007). The procedure used to measure the cross sectional area of each ink color in a given sample was as follows:

- Set Image Scale – Using a known working distance (e.g. the image's scale bar), a reference distance is set in the software. The example shown in Figure 26 is for run combination number 13. The known distance set for the example is 500 µm based on the scale bar. As shown in the imageJ screen dump from Figure 27, the 500 µm distance in the image corresponds to 394.67 pixels. This results in a scale of 0.789 pixels/µm for this image.
- Outline Color Regions - The second step involves creating a free hand "lasso" sketch over the area to be measured. For instance, Figure 26 shows a free hand sketch around the red ink region. The area of the sketch outline is measured in μm^2 by ImageJ using the built-in Analyze function. The process is repeated for the blue and yellow regions. Table 6 shows the areas measured and proportions for Red, Blue and Yellow for trial 13.

Table 6: Proportion of colors for run combination 13

Color	Area under the sketch (μm^2)	Area Fraction
Red	38573	0.21
Blue	32596	0.17
Yellow	120405	0.62
	Total	1.00

CHAPTER 4: RESULTS AND DISCUSSION

Chapter 3 described the experimental setup for flow rate and composition experiments. The results from the experiments are discussed in this chapter. Equations relating ink proportions to the process parameters have been generated using general linear regression analysis in Minitab. The final section of the chapter deals with validating the generated equations using a linear program in AMPL.

4.1 FLOW RATE EXPERIMENTS: RESULTS

The flow rate experiments were carried out to determine the effects of extruder location, pressure, needle position and ink color on the mass flow rate of the inks through the system. Table 1 and Table 2 showed the different factors considered for the experiments and their individual levels. Table 7 shows the p-values for the main effects and two-way interaction effects using full factorial analysis in Minitab. To determine the significance of factors, the p-value of main and interaction effects were compared to commonly used confidence level α of 5%. Comparing the p-value of factors obtained from Table 7 to α, we observe that the main effects of pressure and needle position, and the interaction effect between them are significant. P-values of interaction effects of needle position* ink, the interaction effect of extruder location*needle position and interaction effect of extruder location*ink indicate that they are significant. Since these values are significant, they should be included in our final model. However, the interaction effects plot shown in Figure 28 indicates that these interactions are not significant and are removed from further analysis. The p-value of interaction effect of pressure and needle position is less than α and hence it is significant. It is also verified from the interaction effect plot.

Table 7: Analysis of variance for flow rate sqrt

Source	DF	Seq SS	Adj SS	Adj MS	F	P
Extruder Location	2	0.000018	0.000018	0.000009	0.82	0.442
Pressure	1	0.155992	0.155992	0.155992	14102.66	0.000
Needle Position	1	0.124099	0.124099	0.124099	11219.32	0.000
Ink	2	0.000009	0.000009	0.000004	0.40	0.674
Extruder Location*Pressure	2	0.000055	0.000055	0.000028	2.49	0.089
Extruder Location*Needle Position	2	0.000075	0.000075	0.000038	3.41	0.038
Extruder Location*Ink	4	0.000106	0.000106	0.000027	2.40	0.056
Pressure*Needle Position	1	0.064611	0.064611	0.064611	5841.23	0.000
Pressure*Ink	2	0.000013	0.000013	0.000007	0.59	0.555
Needle Position*Ink	2	0.000082	0.000082	0.000041	3.72	0.028
Error	88	0.000973	0.000973	0.000011		
Total	107	0.346033				
S = 0.00332583 R-Sq = 99.72% R-Sq(adj) = 99.66%						

We can also draw conclusions from the main effects plot and interaction plot shown in Figure 28. To improve the appearance of residual graphs, square root transformation of the mass flow rate data was carried out. From the main effects plot, the mass flow rate obtained is less than the mean mass flow rate as expected at low air pressure and low valve needle position. At high air pressure and high valve needle position, the mass flow rate obtained is greater than the mean mass flow rate. Hence these main effects are significant for mass flow rate. Main effects of ink color and extruder location did not significantly influence the mass flow rate. From the interaction effects plot, the interaction effect of pressure and needle position is significant. All other interaction effects are insignificant.

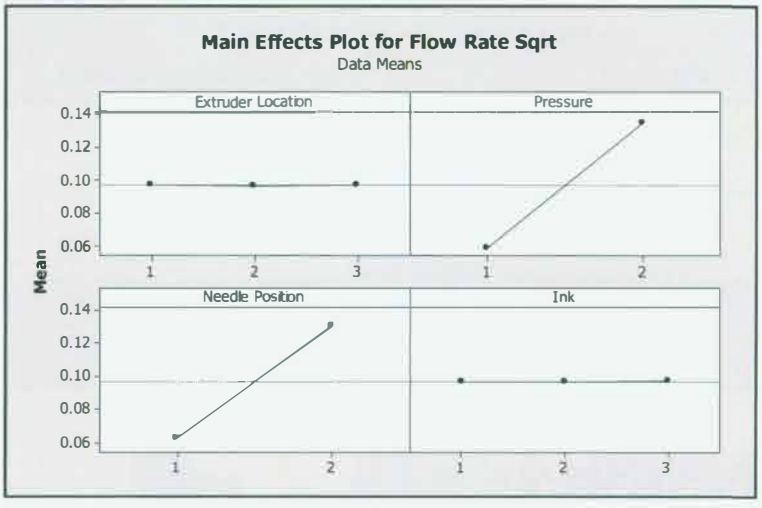

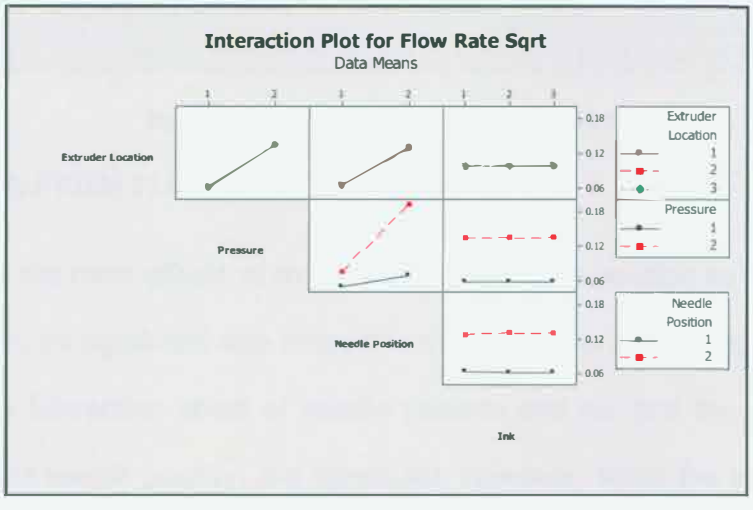

Figure 28: Main and interaction effect for mass flow rate sqrt

Appendix I Figure 37 shows the residual plots for mass flow rate. The residuals from the plot do not indicate normality. As a result, a square root transformation was carried on the mass flow rate. Figure 29 shows the residual plots for the square root of mass flow rate. The normal probability plot indicates that the residuals are normally distributed. The residual versus fits plot indicate that the residuals are randomly distributed about zero. The residual versus order plot does not show any trend. This indicated that the residuals are not affected by the run order.

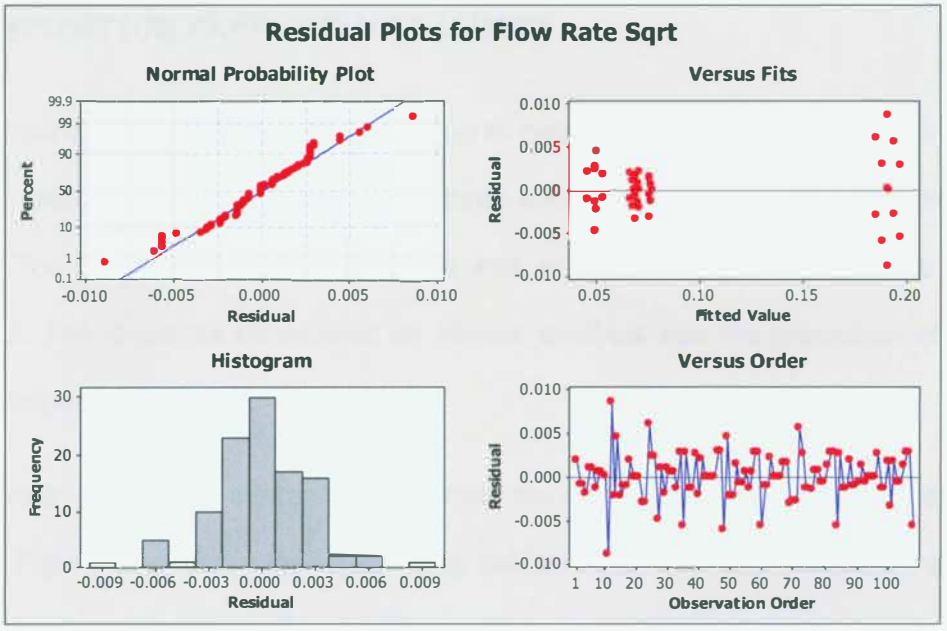

Figure 29: Residual plot for mass flow rate sqrt

4.1.1 DISCUSSION FROM FLOW RATE EXPERIMENTS

In summary, the main effects of air pressure and needle position as well their interaction effects were found to be significant with respect to the mass flow rates of each ink color. The p-value indicates that interaction effect of needle position and ink and the interaction effect of extruder location and needle position are significant. However, since the interaction effect plot does not indicate any practical significance they were not considered for further experiments. As a result of the flow rate experiments, the number of significant factors to study in the composition experiments was reduced to two per extruder location. The extruder location and the ink color are not significant with respect to the mass flow rate. As the three extruder locations have independently controlled air pressure and valve needle position, there were total of 6 factors to be studied. Extruder locations A, B and C, and the ink colors yellow, blue and red were determined to be insignificant with respect to the mass flow rate.

4.2 COMPOSITION EXPERIMENT RESULTS

Final composition experiments were run to determine the effects of needle position and air pressure values on the proportion of the three inks and their mass flow rate in the nScrypt multi-mixer. The cross-section of printed lines was analyzed using the procedure described in Section 3.4.2. The response considered for Minitab analysis was the proportion of yellow, blue and red ink dispensed.

The main effects and interaction plots from the composition experiments are explained in this section. Figure 30 displays the relationship between the main and interaction effects for the proportion of yellow ink. Figure 31 and Figure 32 indicate the relationship between main and interaction effects for blue and red inks respectively.

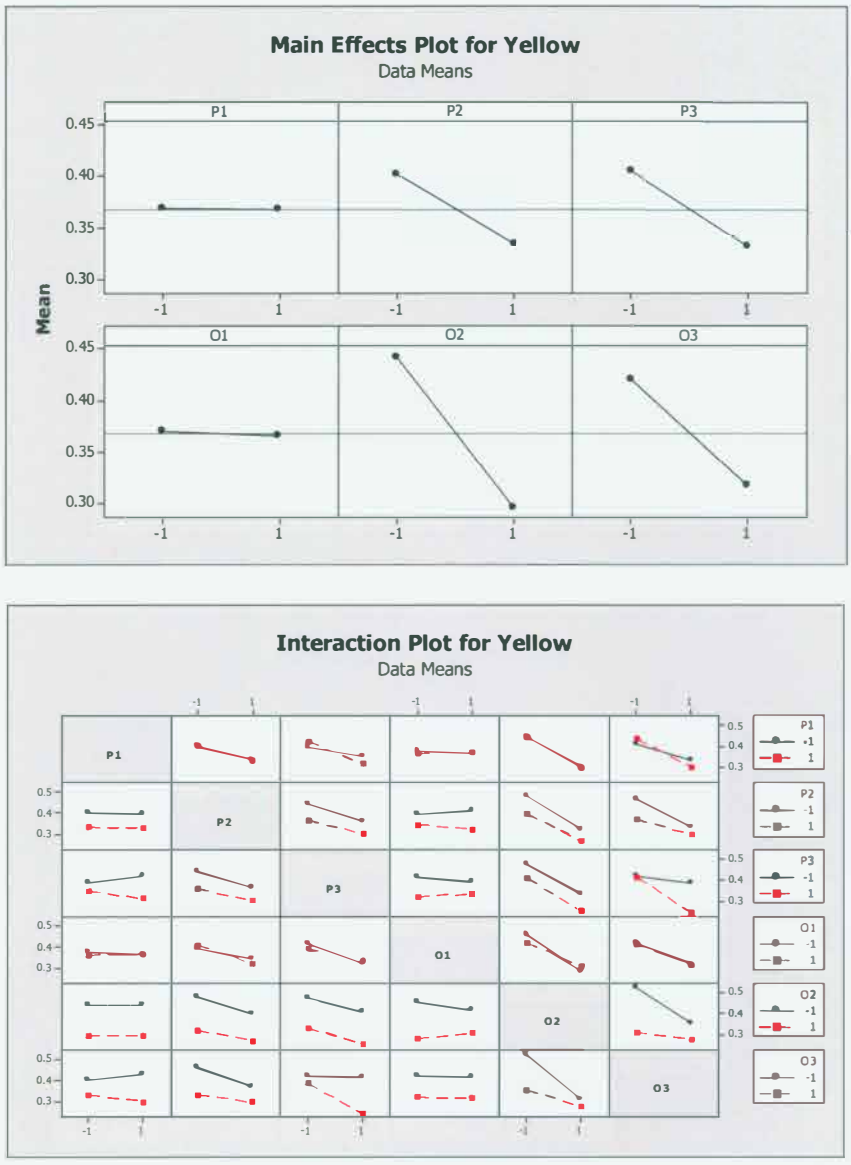

Figure 30: Main and interaction effects for yellow ink

Through this set of experiments, it can be observed that the proportions of inks dispensed is affected mainly by the differential in needle position and air pressure between the ink in location A and the inks in locations B and C. Considering the main effects plot for yellow ink (Figure 30), the low or high values of pressure and needle position for extruder location A do not cause significant deviation from the mean proportions of yellow ink. However, low/ high parametric values at extruder locations B and C (relative to location A) have a significant effect on the proportion of yellow color dispensed.

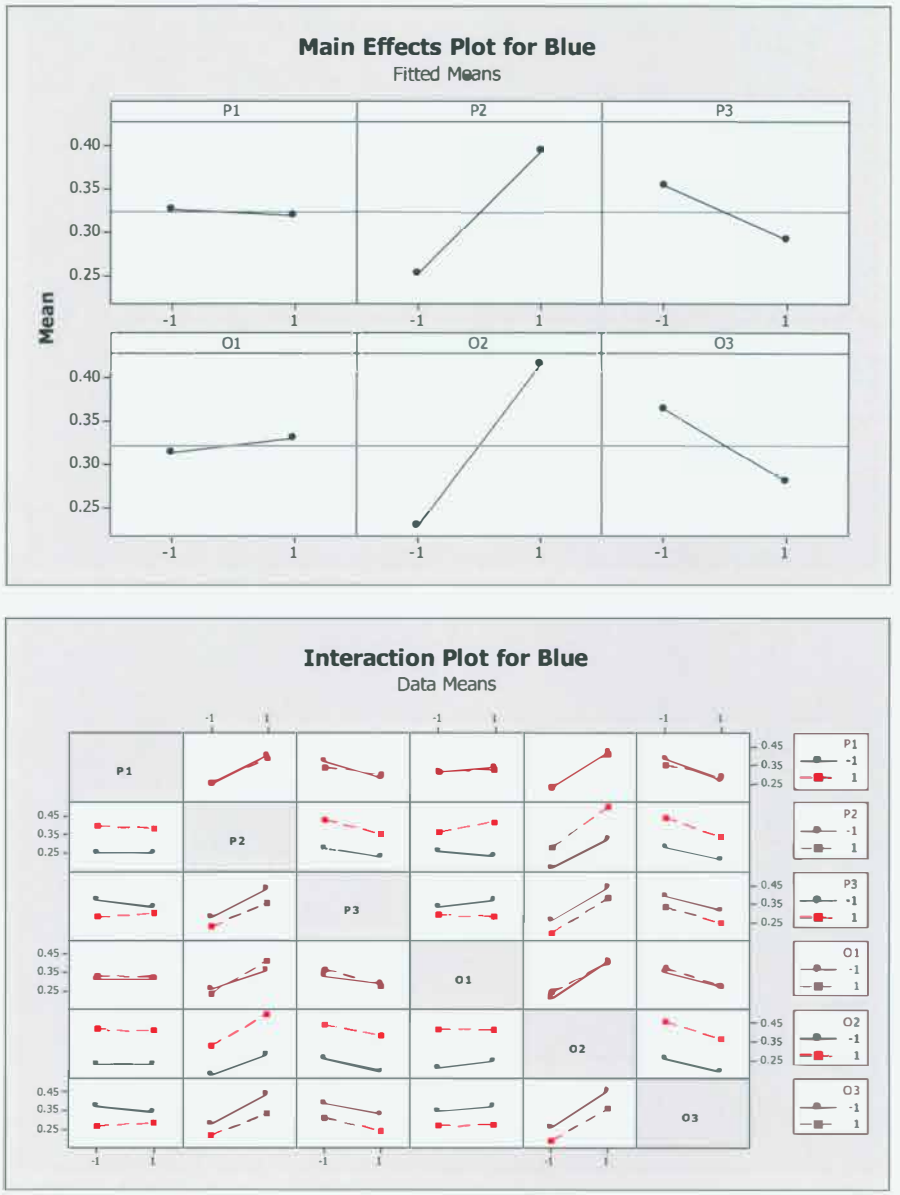

Figure 31: Main and interaction effects for blue ink

For the blue ink loaded in extruder location B, Figure 31 indicates that low Pb, Ob and high value of Pc, Oc values leads to a lower proportion of blue ink with respect to the mean value. At high values for Pb, Ob and low value of Pc, Oc the proportion of blue ink is higher than the mean value. Low/High values of Pa and Oa do not significantly affect proportion of blue ink. These results agree with intuition. A low relative pressure and/or more closed needle position for the blue ink should indeed reduce the relative proportion of blue ink in the dispensed lines.

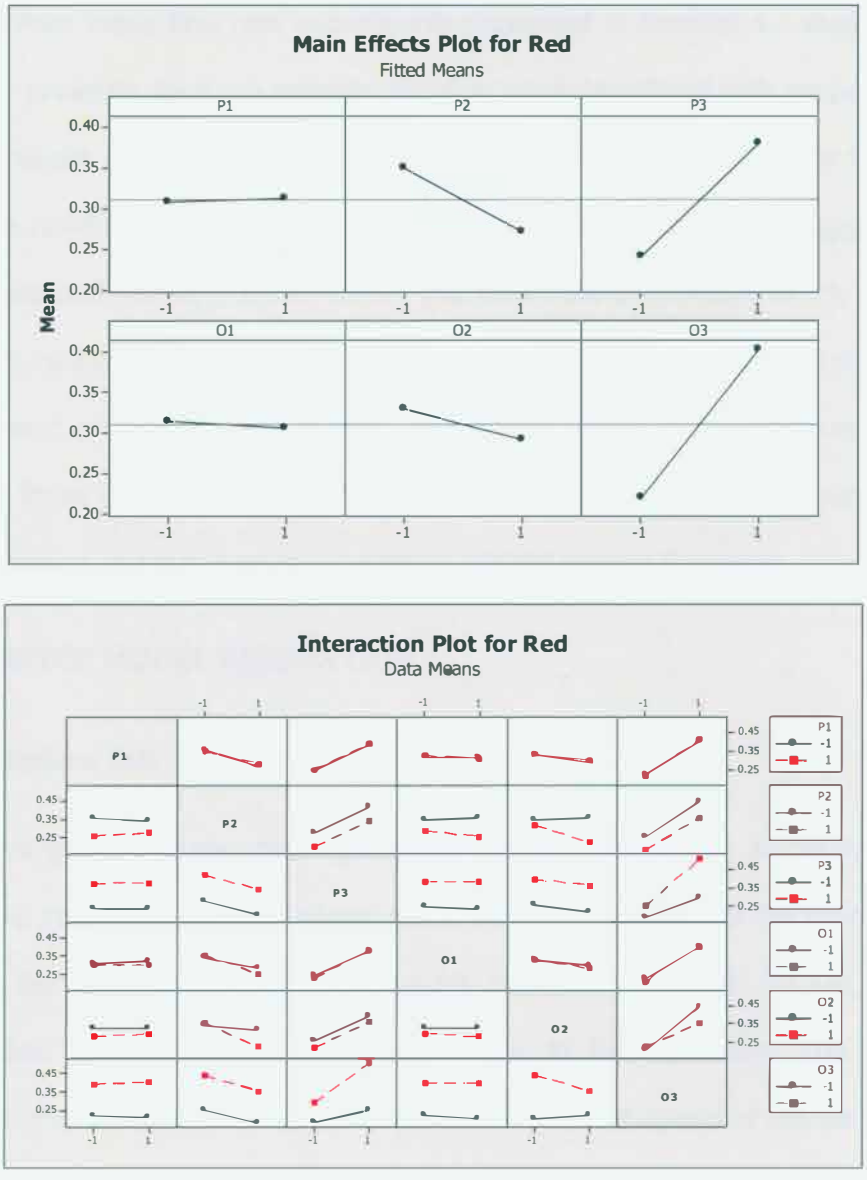

Figure 32: Main and interaction effects for red ink

For red ink loaded in extruder location C, Figure 32 suggests that low values of Pc, Oc and high values of Pb, Ob result in lower proportions of red ink than the mean. At high values of Pc, Oc and low values of Pb, Ob, a higher proportion of red ink with respect to the mean is observed. Low/High values of Pa and Oa do not significantly affect proportion of red ink. As was the case with the blue ink, these findings are logical and agree with intuition.

Results from mass flow rate experiments explained in Section 4.1 showed that needle position and air pressure for each extruder location were significant with respect to mass flow rate. From the results of composition experiments, it is observed that absolute values of factors do not affect the relative proportions of inks dispensed. Rather, it is the differences between the absolute pressure and needle position values that affect the proportions of ink dispensed. This also agrees with intuition. If all pressures and needle positions are equal, then one would expect the flow rates and proportions of the three inks to be equal. If the pressure and/or needle positions for all three valves are then adjusted up or down by the same amount, then the total flow rate may change, but the relative proportions will still remain the same.

4.2.1 PARAMETER MODEL GENERATION

4.2.1.1 Yellow Ink

Using the general linear model generating module in Minitab, an analysis of variance was done for the yellow ink. Table 8 shows the analysis of variance for the proportion of yellow ink. Comparing the p – values with α equal to 0.05, the main effects Pb, Pc, Ob, and Oc as well as the interaction effect between Pc*Oc are found to be significant. The significance of interaction effect Pc*Oc indicates that instead of the differential values of needle position and air pressure at extruder location C, their interaction determines the proportion of yellow ink dispensed. Similarly we would have assumed that the interaction between the differentials of needle position and air pressure at extruder location B is significant. However, the Minitab analysis shows that this interaction effect is not significant and hence is not considered for further analysis. Factors Pa and Oa are not significant for the proportion of yellow ink. From the results, we can conclude that differences in pressure and needle position rather than the actual values play an important role in determining the proportion of yellow ink dispensed. Table 9 tabulates the significant terms and their coefficients used for developing an equation that

explains the relationship between the air pressure and needle position with the proportion of yellow ink (zA). Looking at the p-value for the factors, we observe that Pa, Oa are not significant. However, since the values of Pb, Pc and Ob, Oc are dependent on values of Pa, Oa they have been included in the Equation 1.

Equation 1: Parametric equation for proportion of yellow ink

$$zA = 0.00094\,\mathrm{Pa} + 0.03344\,\mathrm{Pb} + 0.03656\,\mathrm{Pc} + 0.00219\,\mathrm{Oa} + 0.07312\,\mathrm{Ob} + 0.05125\,\mathrm{Oc} - 0.03531\,\mathrm{Pc} * \mathrm{Oc} + 0.36812$$

Table 8: Analysis of Variance for Yellow Ink, using Adjusted SS for Tests

Factor	DF	Seq SS	Adj SS	Adj MS	F	P
Pa	1	0.00006	0.00006	0.00006	0.00	0.945
Pb	1	0.07156	0.07156	0.07156	6.11	0.017
Pc	1	0.08556	0.08556	0.08556	7.30	0.009
Oa	1	0.00031	0.00031	0.00031	0.03	0.873
Ob	1	0.34222	0.34222	0.34222	29.20	0.000
Oc	1	0.16810	0.16810	0.16810	14.31	0.000
Pa*Pb	1	0.00002	0.00002	0.00002	0.00	0.963
Pa*Pc	1	0.01690	0.01690	0.01690	1.44	0.236
Pa*Oa	1	0.00090	0.00090	0.00090	0.08	0.783
Pa*Ob	1	0.00006	0.00006	0.00006	0.00	0.945
Pa*Oc	1	0.01626	0.01626	0.01626	1.39	0.245
Pb*Pc	1	0.00250	0.00250	0.00250	0.21	0.646
Pb*Oa	1	0.00562	0.00562	0.00562	0.48	0.492
Pb*Ob	1	0.00526	0.00526	0.00526	0.45	0.506
Pb*Oc	1	0.01381	0.01381	0.01381	1.18	0.284
Pc*Oa	1	0.00723	0.00723	0.00723	0.62	0.436
Pc*Ob	1	0.00106	0.00106	0.00106	0.09	0.765
Pc*Oc	1	0.07981	0.07981	0.07981	6.81	0.012
Error	45	0.52736	0.52736	0.01172		
Total	63	1.34457				
S = 0.108255	**R-Sq = 60.78%**		**R-Sq(adj) = 45.09%**			

Table 9: Terms for linear model – yellow ink

Factor	Coef	SE Coef
Constant	0.36812	0.01353
Pa	0.00094	0.01353
Pb	0.03344	0.01353
Pc	0.03656	0.01353
Oa	0.00219	0.01353
Ob	0.07312	0.01353
Oc	0.05125	0.01353
Pc*Oc	-0.03531	0.01353

Residual plots for yellow ink are shown in Figure 33; the histogram suggests some skewness in the residuals. But the probability plot shown in Appendix II Figure 38 show the data points follow roughly a straight line and the p-value is greater than 0.05. Hence the residuals are deemed to be normal. The residual versus fits plot indicate that the residuals are randomly distributed about zero. Since the residual versus order plot does not indicate any trend, the residuals are not affected by the run order.

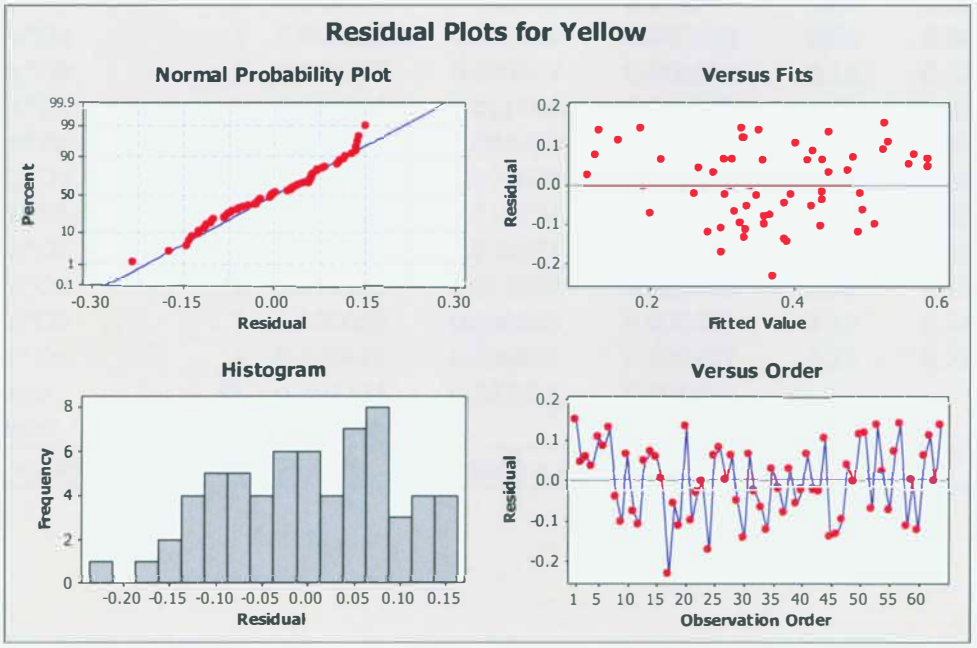

Figure 33: Residual plots for yellow ink

4.2.1.2 Blue ink

Using the general linear model generating module in Minitab, an analysis of variance was done for blue ink. Table 10 shows the analysis of variance for blue ink composition. Comparing the p – values of factors with α equal to 5%, the main effects Pb, Pc, Ob, and Oc are significant. Factors Pa and Oa are not significant for the proportion of blue ink. From the results, we can conclude that differences in the value of pressure and needle position, rather than their absolute values, play an important role in determining the proportion of blue ink dispensed.

Table 10: Analysis of variance for blue ink, using adjusted SS for tests

Factor	DF	Seq SS	Adj SS	Adj MS	F	P
Pa	1	0.000564	0.000564	0.000564	0.09	0.771
Pb	1	0.323477	0.323477	0.323477	48.97	0.000
Pc	1	0.064389	0.064389	0.064389	9.75	0.003
Oa	1	0.004389	0.004389	0.004389	0.66	0.419
Ob	1	0.564377	0.564377	0.564377	85.44	0.000
Oc	1	0.114752	0.114752	0.114752	17.37	0.000
Pa*Pb	1	0.001314	0.001314	0.001314	0.20	0.658
Pa*Pc	1	0.012377	0.012377	0.012377	1.87	0.178
Pa*Oa	1	0.000189	0.000189	0.000189	0.03	0.866
Pa*Ob	1	0.000827	0.000827	0.000827	0.13	0.725
Pa*Oc	1	0.011289	0.011289	0.011289	1.71	0.198
Pb*Pc	1	0.004389	0.004389	0.004389	0.66	0.419
Pb*Oa	1	0.023639	0.023639	0.023639	3.58	0.065
Pb*Ob	1	0.015314	0.015314	0.015314	2.32	0.135
Pb*Oc	1	0.005077	0.005077	0.005077	0.77	0.385
Pc*Oa	1	0.012939	0.012939	0.012939	1.96	0.168
Pc*Ob	1	0.000689	0.000689	0.000689	0.10	0.748
Pc*Oc	1	0.000827	0.000827	0.000827	0.13	0.725
Error	45	0.297233	0.297233	0.006605		
Total	63	1.458048				
S = 0.0812722	**R-Sq = 79.61%**		**R-Sq(adj) = 71.46%**			

Table 11: Terms for linear model – blue ink

Factor	Coef	SE Coef
Constant	0.32266	0.01016
Pa	0.00297	0.01016
Pb	-0.07109	0.01016
Pc	0.03172	0.01016
Oa	-0.00828	0.01016
Ob	-0.09391	0.01016
Oc	0.04234	0.01016

Table 11 provides the significant terms and their coefficients used for developing a parametric equation that explains the relationship between the air pressure and needle position with the proportion of blue ink (zB). Looking at the p-value for the factors, we conclude that Pa, Oa are not significant. However, since the values of Pb, Pc and Ob, Oc are dependent on values of Pa, Oa they have been included in the parametric Equation 2.

Equation 2: Parametric equation for proportion of blue ink

$$\boldsymbol{zB} = 0.00297\ Pa - 0.07109\ Pb + 0.03172\ Pc - 0.00828\ Oa - 0.09391\ Ob + 0.04234\ Oc + 0.32266$$

Residual plots for blue ink are shown in Figure 34; the histogram suggests some skewness. The probability plot shown in Appendix II Figure 39 indicates that the data points roughly follow a straight line, and the p-value is greater than 0.05. Hence the residuals are deemed to be normal. The residual versus fits plot indicates that the residuals are randomly distributed about zero. The residual versus order plot does not show any trend. This indicates that the residuals are not affected by the run order.

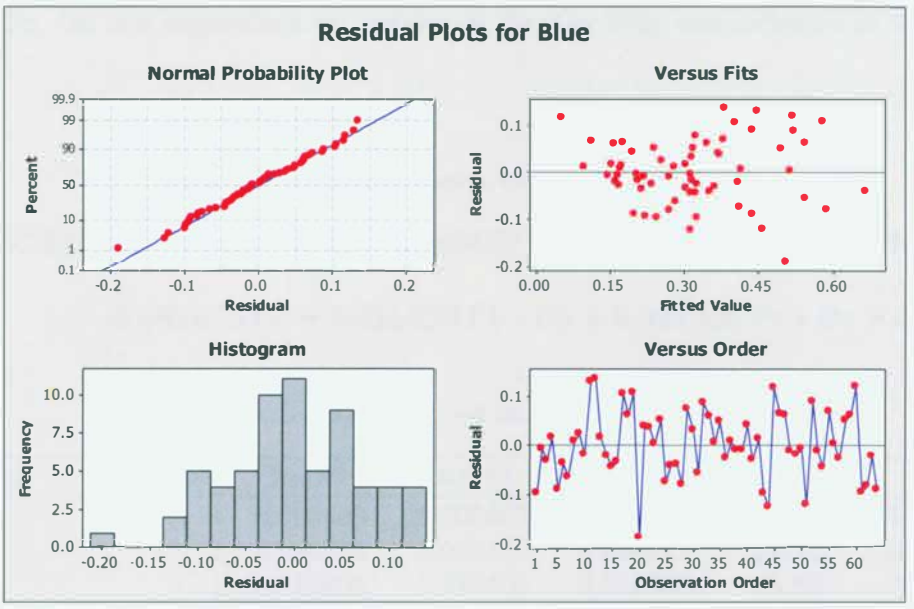

Figure 34: Residual plots for blue ink

4.2.1.3 Red ink

Using the general linear model generating module in Minitab, an analysis of variance was done for the proportion of red ink. Table 12 shows the analysis of variance for the proportion of red ink. Comparing the p – values of factors with α equal to 0.05, we have main effects Pb, Pc, Ob, and Oc as well as interaction effects of Pb*Ob and Pc*Oc are significant. Factors Pa and Oa are not significant for the proportion of red ink. From the results, we can conclude that rather than the absolute value, differentials in the pressure and needle position and their interaction effects mainly affect the proportion of red ink dispensed. From the interaction effect plot shown in Figure 32, we can conclude that the interaction effects are mainly significant. The significance of interaction effects indicate that the proportion of red dispensed is not dependent on the differential value of either needle position or air pressure, but the interaction of those values at extruder locations B and C. Table 13 provides the significant terms and their coefficients to develop a parametric equation that explains the relationship between the air pressure and needle position with the proportion of red ink (zC). Looking at p value for the factors, we conclude that Pa, Oa are not significant. However, since the values of

Pb, Pc and Ob, Oc are dependent on values of Pa, Oa they are included in the parametric Equation 2.

Equation 3: Parametric equation for proportion of red ink

$$zC = -0.0025\,Pa + 0.039375\,Pb - 0.069687\,Pc + 0.004375\,Oa + 0.01906\,Ob$$
$$- 0.091875\,Oc - 0.026250\,Pb * Ob + 0.037500\,Pc * Oc + 0.310937$$

Table 12: Analysis of variance for red ink, using adjusted SS for tests

Factor	DF	Seq SS	Adj SS	Adj MS	F	P
Pa	1	0.000400	0.000400	0.000400	0.08	0.773
Pb	1	0.099225	0.099225	0.099225	20.91	0.000
Pc	1	0.310806	0.310806	0.310806	65.50	0.000
Oa	1	0.001225	0.001225	0.001225	0.26	0.614
Ob	1	0.023256	0.023256	0.023256	4.90	0.032
Oc	1	0.540225	0.540225	0.540225	113.84	0.000
Pa*Pb	1	0.002756	0.002756	0.002756	0.58	0.450
Pa*Pc	1	0.000025	0.000025	0.000025	0.01	0.942
Pa*Oa	1	0.000756	0.000756	0.000756	0.16	0.692
Pa*Ob	1	0.000625	0.000625	0.000625	0.13	0.718
Pa*Oc	1	0.001056	0.001056	0.001056	0.22	0.639
Pb*Pc	1	0.000025	0.000025	0.000025	0.01	0.942
Pb*Oa	1	0.008556	0.008556	0.008556	1.80	0.186
Pb*Ob	1	0.044100	0.044100	0.044100	9.29	0.004
Pb*Oc	1	0.001056	0.001056	0.001056	0.22	0.639
Pc*Oa	1	0.001600	0.001600	0.001600	0.34	0.564
Pc*Ob	1	0.000306	0.000306	0.000306	0.06	0.801
Pc*Oc	1	0.090000	0.090000	0.090000	18.97	0.000
Error	45	0.213544	0.213544	0.004745		
Total	63	1.339544				
S = 0.0688870	**R-Sq = 84.06%**		**R-Sq(adj) = 77.68%**			

Table 13: Terms for linear model – red ink

Factor	Coef	SE Coef
Constant	0.310937	0.008611
Pa	-0.002500	0.008611
Pb	0.039375	0.008611
Pc	-0.069687	0.008611
Oa	0.004375	0.008611
Ob	0.019062	0.008611
Oc	-0.091875	0.008611
Pb*Ob	-0.026250	0.008611
Pc*Oc	0.037500	0.008611

Residual plots for red ink are as shown in Figure 35. The histogram shows that the residuals are normally distributed. The residual versus fits plot indicate that the residuals are randomly distributed about zero. The residual versus order plot do not show any observable trend. This indicates that the residuals are not affected by the run order.

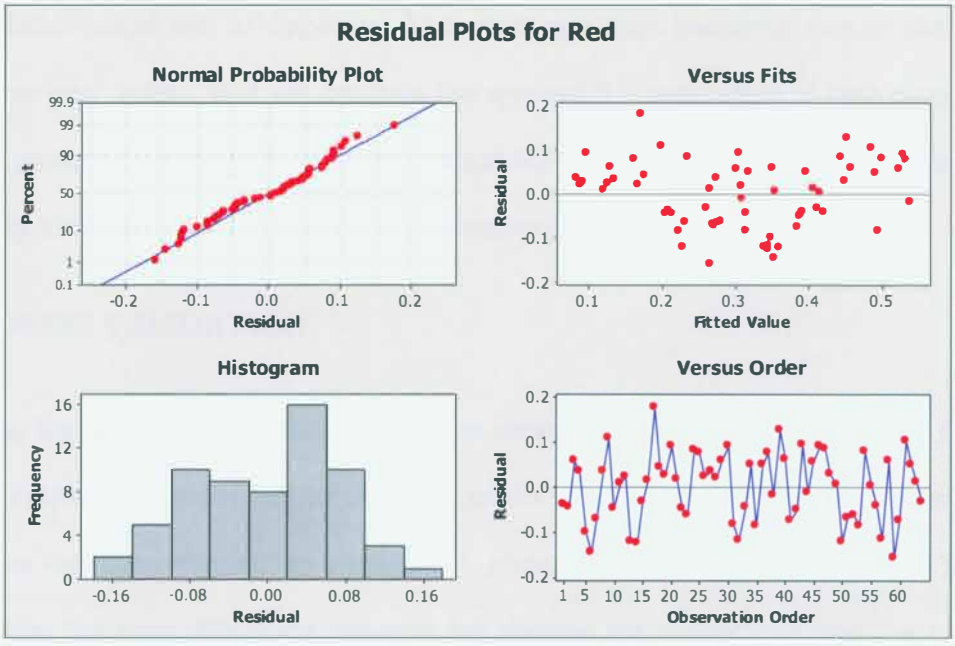

Figure 35: Residual plots for red ink

4.2.2 DISCUSSION OF COMPOSITION EXPERIMENTS

From the results of parameter model generation discussed in Section 4.2.1 it was concluded that the absolute values of parameters do not particularly affect the proportion of inks dispensed within the parameter range studied. They primarily affect the total mass flow rate of composite ink dispensed. The relative proportions of inks dispensed are primarily dictated by the magnitude of the differences between needle position and air pressures for valves A, B, and C. The parametric equations governing the proportions of inks dispensed were determined by creating a general linear model within Minitab. The equations thus obtained from the general linear model are shown in Equation 1, Equation 2 and Equation 3. The boundary conditions for each parameter are as follows:

Table 14: Boundary limits for significant process parameters

Parameter	Boundary Limits	
	Low Value	High Value
Pressure (in volts)	0.90	1.50
Needle Position (mm)	1.48	1.60

In practice, a technician or engineer using this process knows the relative proportions of inks that he/she would like to dispense. The challenge then becomes one of determining the process parameter values that will produce the desired the proportion of inks dispensed. In an attempt to provide this information, the proportion equations were solved using a linear programming formulation with the boundary conditions given in Table 14.

4.3 PROCESS VALIDATION

Using the equations developed from the designed experiments, an AMPL program was created for validation of experimental data. Appendix I show the AMPL program created to solve the equations for experimental run number 10, chosen at random. The objective function was set to minimize the total difference between the desired ink proportions and the calculated ink proportions. For the linear program, the calculated proportions of inks A, B and C are considered as zA, zB and zC. These ink proportions are calculated using the three parametric equations developed. The desired proportions of inks A, B and C are considered as zAd, zBd, zCd. The design engineer decides these values, and they are used to solve the linear program to obtain the required parameter values. The linear program developed is as shown below.

Minimize: (zA - zAd) + (zB - zBd) + (zC - zCd).

subject to propA: zA= 0.00094*Pa + 0.03344*Pb + 0.03656*Pc + 0.00219*Oa + 0.07312*Ob + 0.05125*Oc - 0.03531*(Pc*Oc) + 0.36812;

subject to propB: zB = 0.00297*Pa - 0.07109*Pb + 0.03172*Pc - 0.00828*Oa - 0.09391*Ob + 0.04234*Oc + 0.32266;

subject to probC: zC = -0.0025*Pa + 0.039375*Pb - 0.069687*Pc + 0.004375*Oa + 0.01906*Ob - 0.091875*Oc - 0.026250*(Pb*Ob) + 0.037500*(Pb*Ob) + 0.310937;

subject to Pa_limit: 1.1 <= Pa <= 1.3;
subject to Pb_limit: -0.2 <= Pb <= 0.2;
subject to Pc_limit: -0.2 <= Pc <= 0.2;
subject to Oa_limit: 1.52 <= Oa <= 1.56;
subject to Ob_limit: -0.04 <= Ob <= 0.04;
subject to Oc_limit: 0.04 <= Oc <= 0.04;
subject to sum_limit: zA + zB + zC = 1;
subject to prop_A_desired: zAd = 0.65;
subject to prop_B_desired: zBd = 0.13;
subject to prop_C_desired: zCd = 0.26;

The solution window using the MINOS solver for experimental run # 10 is shown in Figure 36. Table 15 shows the experimental parameters for runs # 10, 30, 46, 60, all chosen at random, and the parameters obtained after solving the linear program using AMPL. Note in this case that pressures Pa, Pb, and Pc are measured in regulator voltage that produces the desired pressure, and Oa, Ob and Oc are measured in millimeters.

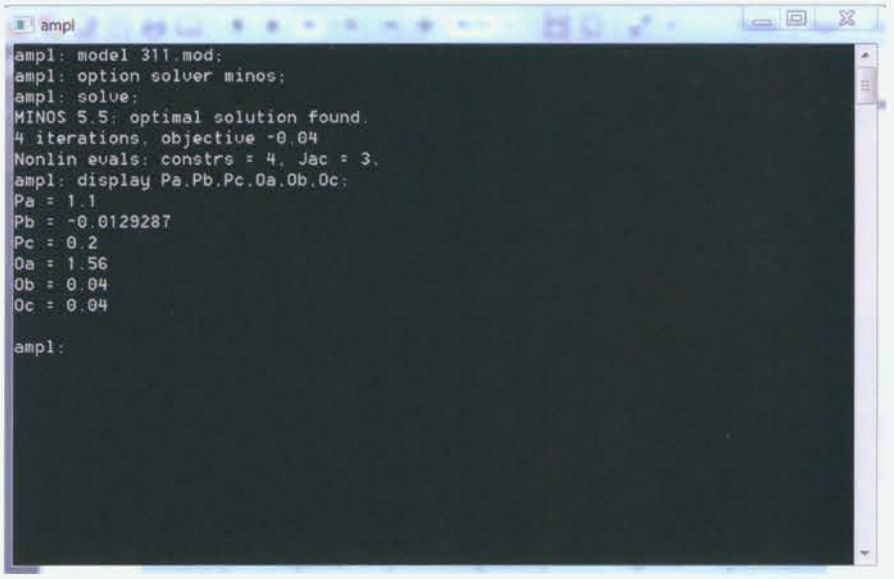

Figure 36: AMPL program Solved Using minos solver

Table 15: Comparison of parameters between experimental run and AMPL program

	Run # 10		Run # 30		Run # 60		Run # 46	
	Experiment	From AMPL	Experiment	From AMPL	Experiment	From AMPL	Experiment	From AMPL
Pa	1.30	1.10	1.30	1.10	1.30	1.10	1.30	1.10
Pb	1.10	1.08	1.10	1.08	1.50	0.90	1.10	0.90
Pc	1.10	1.3	1.50	1.30	1.10	1.30	1.50	1.30
Oa	1.56	1.56	1.56	1.56	1.56	1.56	1.56	1.56
Ob	1.52	1.60	1.6	1.60	1.60	1.60	1.52	1.59
Oc	1.52	1.60	1.52	1.60	1.60	1.60	1.60	1.59

It can be seen from Table 15 that the values obtained from the linear program trend toward the experimental values, but that there is certainly room for improvement.

Another method used to validate the experimental results involved printing inks using the same procedures as was used for the composition experiments. The parameter values used are shown in Table 16. These values are different from any values that were used to carry out the composition experiments. The proportions of inks obtained using the new sets of parameters were measured using the procedure explained in Section 3.4.2. The parametric model defined by Equation 1, Equation 2 and Equation 3 was solved, and the difference between the proportions of inks was noted. Table 16 and Table 17 describe the proportions of inks obtained from the experiment and the equations respectively for the each run combination. The percent deviation between the actual proportion of inks obtained and the proportion of inks predicted by the modeled equations is less than 0.10%.

Table 16: Results of validation experiments for run combination A

Parametric Values	Pa	Pb	Pc	Oa	Ob	Oc
	1.50	1.30	1.30	1.48	1.48	1.48
Proportions	***From Experiments***		***From Equations***		***Percent Deviation***	
Yellow (Ink A)	0.64		0.60		0.04%	
Blue (Ink B)	0.19		0.19		0.00%	
Red (Ink C)	0.17		0.21		-0.04%	

Table 17: Results of validation experiments for run combination B

Parametric Values	Pa	Pb	Pc	Oa	Ob	Oc
	1.10	1.10	1.10	1.60	1.48	1.48
Proportions	***From Experiments***		***From Equations***		***Percent Deviation***	
Yellow (Ink A)	0.62		0.55		0.07%	
Blue (Ink B)	0.18		0.23		-0.05%	
Red (Ink C)	0.20		0.22		-0.02%	

CHAPTER 5: SUMMARY AND CONCLUSIONS

5.1 SUMMARY

Functionally graded materials have tremendous applications in various fields, right from biomedical to aerospace industries. In biomedical applications, we have seen that FGM's are widely used as scaffolds for bone implants. In the aerospace industry, FGM's reduce weight and increase efficiency by providing a thermal barrier shield which gradually changes its composition. FGM's are now also being used to manufacture solid oxide fuel cells. Considering the wide range of applications for functionally graded materials, a variety of manufacturing methods have been developed.

Direct write printing is a relatively new type of method developed to manufacture functionally graded materials. Direct-write printing is conceptually similar to ink jet printing in the sense that one or more materials are deposited from a nozzle and printed layer by layer to create a 3D model.

In order to print FGM's using multiple materials; variations in the quantities of multiple inks must be accurately controlled. A study was carried out using an nScrypt multi-mix dispensing tool with three acrylic inks. Initial experiments demonstrated that for a particular ink, the relative needle position and air pressure are the primary factors that affect the mass flow rate and proportions of ink dispensed. The minimum needle opening required for material flow has been determined experimentally. Below this particular value of needle position (1.48 mm), no ink flow was obtained irrespective of any amount of air pressure applied. At needle position values greater than 1.60 mm, there was no effect on the mass flow rate of the ink. At high values of air pressure (>30 psi) and high value of valve needle position (>1.60 mm), the mass flow was too high to obtain a stable printed line.

The main and interaction effects plot obtained from the 2-level experiment involving six factors indicated that the pressure and needle position differentials played a major role in determining the relative proportions of inks dispensed.

The equations obtained from the general linear model explain the relationship between the significant multi-mixer parameters. The yellow, blue, and red inks correspond to extruder locations A, B and C. The equations obtained are as follows:

$$\boldsymbol{Proportion\ of\ A}$$

$$= 0.00094\,Pa + 0.03344\,Pb + 0.03656\,Pc + 0.00219\,Oa + 0.07312\,Ob + 0.05125\,Oc - 0.03531\,Pc * Oc + 0.36812$$

$$\boldsymbol{Proportion\ of\ B}$$

$$= 0.00297\,Pa - 0.07109\,Pb + 0.03172\,Pc - 0.00828\,Oa - 0.09391\,Ob + 0.04234\,Oc + 0.32266$$

$$\boldsymbol{Proportion\ of\ C}$$

$$= -0.0025\,Pa + 0.039375\,Pb - 0.069687\,Pc + 0.004375\,Oa + 0.01906\,Ob - 0.091875\,Oc - 0.026250\,Pb * Ob + 0.037500\,Pb * Ob + 0.310937$$

The equations obtained from the designed experiments were formulated as a linear program using the AMPL programming language, and were then solved using MINOS solver. The aim here is to allow engineers to input the desired ink ratios and to have the LP's output provide guidance on process parameter values that will produce the desired ink ratios. Two sets of parameters were selected, and a validation experiment was executed. The proportions of inks obtained from the experiments and by solving the equations were compared. The percent deviation between the two values was less than 0.10%.

5.2 FUTURE WORK

5.2.1 INK USED

The current work uses water based yellow, blue, and red acrylic inks in the multi-mixer. However, factors such as the size of the ink particles and the solid loading fraction can affect the ink rheology and the resulting proportions of materials dispensed for given process parameters. As the scientific understanding of multi-material ink dispensing improves, model complexity can expand to encompass other factors such as the properties of the inks being dispensed.

The current work was used as a model study to understand the relationship between the significant factors and the proportion of inks dispensed. The experimental procedures developed here can now be applied for functional materials and inks for specific FGM applications. As some inks used to print functionally graded materials have similar color and cannot be distinguished via color analysis, a more suitable method will need to be developed to accurately measure proportions of inks dispensed.

Ink rheology and ink particle size for different ink affect the mass flow rate of the ink. The nozzle diameters available for printing FGMs range from 12.5 μm to 125 μm. The nozzle diameter will affect the shear rate of the inks and should also be included as a possible factor affecting mass flow rate. If these factors are added in the parametric equations, it may be possible to accurately predict the parameter values for a range of inks based on their rheological properties.

5.2.2 COLOR MIXING USING THE MULTI-MIXER

The current work only deals with co-extrusion of three materials having the same properties and different colors so that they could be easily distinguished. The machine parameters involving mixing motors were not considered a part of the experiments. The full

capability of the multi-mixer can be used to print a graded composition such as the rainbow pattern as shown in Figure 17(a). To achieve this type of pattern, a study of the effects of mixing motor parameters on the quality of ink mixing need to be carried out. The properties that may affect the mixing quality have been described below. Future work needs to consider these effects on the mixing quality.

a. Ink viscosity
b. Mixing motor speed (RPM)
c. Feed rate
d. Nozzle diameter
e. Motion delay
f. Ink particle size.

5.3 CONCLUSION

This thesis work determined the parameters influencing the mass flow rate and proportion of inks dispensed via a three-valve micro-extrusion process. We have seen that for a given ink, the air pressure and needle position primarily influence the mass flow rate. The differentials in pressure and needle position primarily affect the proportion of inks dispensed. The parametric equations developed by the designed experiments can determine the values of parameters required to achieve the desired ink proportions.

REFERENCES

Alexandrescu, R., Crunteanu, A., Morjan, R. E., Morjan, I., Rohmund, F., Falk, L. K. L., Huisken, F. (2003). Synthesis of carbon nanotubes by CO2-laser-assisted chemical vapour deposition. *Infrared Physics & Technology, 44*(1), 43-50. doi: 10.1016/S1350-4495(02)00158-5

Calvert, Paul. (2001). Inkjet Printing for Materials and Devices. *Chemistry of Materials, 13*(10), 3299-3305. doi: 10.1021/cm0101632

Cesarano, J. Ill, King, B.H., & Denham, H.B. (1998 Dec 01). *Recent developments in robocasting of ceramics and multimaterial deposition*. Paper presented at the Solid freeform fabrication symposium, Austin, TX (United States).

Chenglin, Chu, Jingchuan, Zhu, Zhongda, Yin, & Shidong, Wang. (1999). Hydroxyapatite-Ti functionally graded biomaterial fabricated by powder metallurgy. *Materials Science and Engineering A, 271*(1-2), 95-100. doi: Doi: 10.1016/s0921-5093(99)00152-5

Chung, Haseung, & Das, Suman. (2006). Processing and properties of glass bead particulate-filled functionally graded Nylon-11 composites produced by selective laser sintering. *Materials Science and Engineering: A, 437*(2), 226-234. doi: DOI: 10.1016/j.msea.2006.07.112

Collins, Tony J. (July 2007). ImageJ for microscopy. *BioTechniques, 43*, S25-S30.

Cooley, William G. (2005). *Application of Functionally graded material in Aircraft Structures.* (Masters of Science), Air Force Institute of Technology, Ohio. (AFIT/GAE/ENY/05-M04)

Domack, M. S., & Baughman, J. M. (2005). Development of nickel-titanium graded composition components. *Rapid Prototyping Journal, 11*(1), 41-51.

Dongjiang Xu, Patrick Clark, Bo Li, Kenneth H. Church. (2009). Vertical Interconnects for Stacked Die using Micro Dispensing. Orlando, FL: nScrypt, Inc.

Erdogan, F. (1995). Fracture mechanics of functionally graded materials. *Composites Engineering, 5*(7), 753-770. doi: Doi: 10.1016/0961-9526(95)00029-m

Gibson, Ian, Rosen, David W., & Stucker, Brent. (2009). *Additive Manufacturing Technologies: Rapid Prototyping to Direct Digital Manufacturing* (1 ed.): Springer.

Ginger, David S., Zhang, Hua, & Mirkin, Chad A. (2004). The Evolution of Dip-Pen Nanolithography. *Angewandte Chemie International Edition, 43*(1), 30-45. doi: 10.1002/anie.200300608

Göransson, Peter. (2008). Tailored acoustic and vibrational damping in porous solids - Engineering performance in aerospace applications. *Aerospace Science and Technology, 12*(1), 26-41. doi: DOI: 10.1016/j.ast.2007.10.007

Hon, K. K. B., Li, L., & Hutchings, I. M. (2008). Direct writing technology--Advances and developments. *CIRP Annals - Manufacturing Technology, 57*(2), 601-620. doi: DOI: 10.1016/j.cirp.2008.09.006

Kawasaki, A., & Watanabe, R. (2002). Thermal fracture behavior of metal/ceramic functionally graded materials. *Engineering Fracture Mechanics, 69*(14-16), 1713-1728. doi: Doi: 10.1016/s0013-7944(02)00054-1

Khatri-Chhetri, Prasanna. (2011). *A Novel Approach to Engineering Structures of a Solid Oxide Fuel Cell: 3D Direct Write Technology*. (Masters of Science), Rochester Institute of Technology, Rochester, NY.

Kim, Chung-Soo, Ahn, Sung-Hoon, & Jang, Dong-Young. (2012). Review: Developments in micro/nanoscale fabrication by focused ion beams. *Vacuum, 86*(8), 1014-1035. doi: 10.1016/j.vacuum.2011.11.004

Kim, K. H., Moldovan, N., & Espinosa, H. D. (2005). A nanofountain probe with sub-100 nm molecular writing resolution. *Small, 1*(6), 632-635.

Kim, W. J., & Sa, Y. K. (2006). Micro-extrusion of ECAP processed magnesium alloy for production of high strength magnesium micro-gears. *Scripta Materialia, 54*(7), 1391-1395. doi: 10.1016/j.scriptamat.2005.11.066

Kumar, S. (2010). Development of Functionally Graded Materials by Ultrasonic Consolidation. *CIRP Journal of Manufacturing Science and Technology, In Press, Corrected Proof*. doi: DOI: 10.1016/j.cirpj.2010.07.006

Kumar, Sanjay. (2003). Selective laser sintering: A qualitative and objective approach. *JOM Journal of the Minerals, Metals and Materials Society, 55*(10), 43-47. doi: 10.1007/s11837-003-0175-y

Li, B., Clark, P. A., & Church, K. H. (2007). *Robust Direct-Write Dispensing Tool and Solutions for Micro/Meso-Scale Manufacturing and Packaging*. Paper presented at the ASME 2007 International Manufacturing Science and Engineering Conference

Li B., Roy Dutta, C.M. Smith,P.A. Clark,K.H. Church. (2007). *A ROBUST TRUE DIRECT-PRINT TECHNOLOGY FOR TISSUE ENGINEERING*. Paper presented at the International Manufacturing Science And Engineering Conference, Atlanta, Georgia, USA.

Li, L., Saedan, M., Feng, W., Fuh, J. Y. H., Wong, Y. S., Loh, H. T., Lu, L. (2009). Development of a multi-nozzle drop-on-demand system for multi-material dispensing. *Journal of Materials Processing Technology, 209*(9), 4444-4448. doi: DOI: 10.1016/j.jmatprotec.2008.10.040

Miranda, Pedro, Saiz, Eduardo, Gryn, Karol, & Tomsia, Antoni P. (2006). Sintering and robocasting of β-tricalcium phosphate scaffolds for orthopaedic applications. *Acta Biomaterialia, 2*(4), 457-466. doi: 10.1016/j.actbio.2006.02.004

Miyamoto, Y., Kaysser, W. A., Rabin, B.H., Kawasaki, A., & Ford, R.G. (1999). *Functionally graded materials: design, processing, and applications* (1 ed.): Springer.

Piqué , Alberto. (2010). Laser Transfer Techniques for Digital Microfabrication. *Laser Precision Microfabrication, 135*, 259-291. doi: 10.1007/978-3-642-10523-4_11

Pompe, W., Worch, H., Epple, M., Friess, W., Gelinsky, M., Greil, P., Schulte, K. (2003). Functionally graded materials for biomedical applications. *Materials Science and Engineering A, 362*(1-2), 40-60. doi: Doi: 10.1016/s0921-5093(03)00580-x

Puippe, J. C., Acosta, R. E., & Von Gutfeld, R. J. (1981). Investigation of Laser Enhanced Electroplating Mechanisms. *Journal of the Electrochemical Society, 128*, 2539.

Pál, Edit, Kun, Robert, Schulze, Christina, Zöllmer, Volker, Lehmhus, Dirk, Bäumer, Marcus, & Busse, Matthias. (2012). Composition-dependent sintering behaviour of chemically synthesised CuNi nanoparticles and their application in aerosol printing for preparation of conductive microstructures. *Colloid & Polymer Science, 290*(10), 941-952. doi: 10.1007/s00396-012-2612-3

Salaita, Khalid, Wang, Yuhuang, & Mirkin, Chad A. (2007). Applications of dip-pen nanolithography. *Nat Nano, 2*(3), 145-155.

Sankar, B. V. (2001). An elasticity solution for functionally graded beams. *Composites Science and Technology, 61*(5), 689-696. doi: Doi: 10.1016/s0266-3538(01)00007-0

Smay, J.E., Gratson, G.M., Shepherd, R.F., Cesarano, J. and Lewis, J.A. (2002). Directed Colloidal Assembly of 3D Periodic Structures. *Advanced Materials, 14*(18), 1279-1283.

Stuecker, John N., Cesarano Iii, Joseph, & Hirschfeld, Deidre A. (2003). Control of the viscous behavior of highly concentrated mullite suspensions for robocasting. *Journal of Materials Processing Technology, 142*(2), 318-325. doi: 10.1016/S0924-0136(03)00586-7

Su, B., & Choy, K. L. (2000). Microstructure and optical properties of CdSe thin films by electrostatic assisted aerosol jet deposition method. *Journal of Materials Science Letters, 19*(20), 1859-1861. doi: 10.1023/A:1006723229844

Tan, K. H., Chua, C. K., Leong, K. F., Cheah, C. M., Cheang, P., Abu Bakar, M. S., & Cha, S. W. (2003). Scaffold development using selective laser sintering of polyetheretherketone–hydroxyapatite biocomposite blends. *Biomaterials, 24*(18), 3115-3123. doi: 10.1016/S0142-9612(03)00131-5

Von Gutfeld, R. J., & Romankiw, L. T. (1982). Laser Enhanced Plating. *Gold Bull., 15*(4), 120-123.

Wang, X. C., Zheng, H. Y., & Lim, G. C. (2002). Laser induced copper electroless plating on polyimide with Q-switch Nd:YAG laser. *Applied Surface Science, 200*(1–4), 165-171. doi: 10.1016/S0169-4332(02)00850-4

Yoshimi, Watanabe, & Hisashi, Sato. (2011). Review Fabrication of Functionally Graded Materials under a Centrifugal Force.

Young, D., Sukeshini, A. M., Cummins, R., Xiao, H., Rottmayer, M., & Reitz, T. (2008). Ink-jet printing of electrolyte and anode functional layer for solid oxide fuel cells. *Journal of Power Sources, 184*(1), 191-196. doi: 10.1016/j.jpowsour.2008.06.018

Zhao, J., Cao, W., Ge, C., Tan, Y., Zhang, Y., & Fei, Q. (2009). Research on laser engineered net shaping of thick-wall nickel-based alloy parts. *Rapid Prototyping Journal, 15*(1), 24-28.

Zhu, Jingchuan, Lai, Zhonghong, Yin, Zhongda, Jeon, Jaeho, & Lee, Sooyoung. (2001). Fabrication of ZrO2-NiCr functionally graded material by powder metallurgy. *Materials Chemistry and Physics, 68*(1-3), 130-135. doi: Doi: 10.1016/s0254-0584(00)00355-2

APPENDIX I

AMPL program for run 10:

```
var Pa;
var Pb;
var Pc;
var Oa;
var Ob;
var Oc;
var zA;
var zB;
var zC;
var zAd;
var zBd;
var zCd;

minimize diff: (zA - zAd) + (zB - zBd) + (zC - zCd);


subject to propA: zA= 0.00094*Pa +  0.03344*Pb + 0.03656*Pc + 0.00219*Oa + 0.07312*Ob +
0.05125*Oc - 0.03531*(Pc*Oc) + 0.36812;

subject to propB: zB = 0.00297*Pa - 0.07109*Pb + 0.03172*Pc - 0.00828*Oa - 0.09391*Ob + 0.04234*Oc
+ 0.32266;

subject to probC: zC = -0.0025*Pa + 0.039375*Pb - 0.069687*Pc + 0.004375*Oa + 0.01906*Ob -
0.091875*Oc - 0.026250*(Pb*Ob) + 0.037500*(Pb*Ob) + 0.310937;

subject to Pa_limit: 0.7 <= Pa <= 1.6;
subject to Pb_limit: 0.7 <= Pb <= 1.6;
subject to Pc_limit: 0.7 <= pC <= 1.6;
subject to Oa_limit: 1.48 <= Oa <= 1.7;
subject to Ob_limit: 1.48 <= Ob <= 1.7;
subject to Oc_limit: 1.48 <= Oc <= 1.7;
subject to sum_limit: zA + zB + zC = 1;
subject to prop_A_desired: zAd = 0.65;
subject to prop_B_desired: zBd = 0.14;
subject to prop_C_desired: zCd = 0.21;
```

APPENDIX II

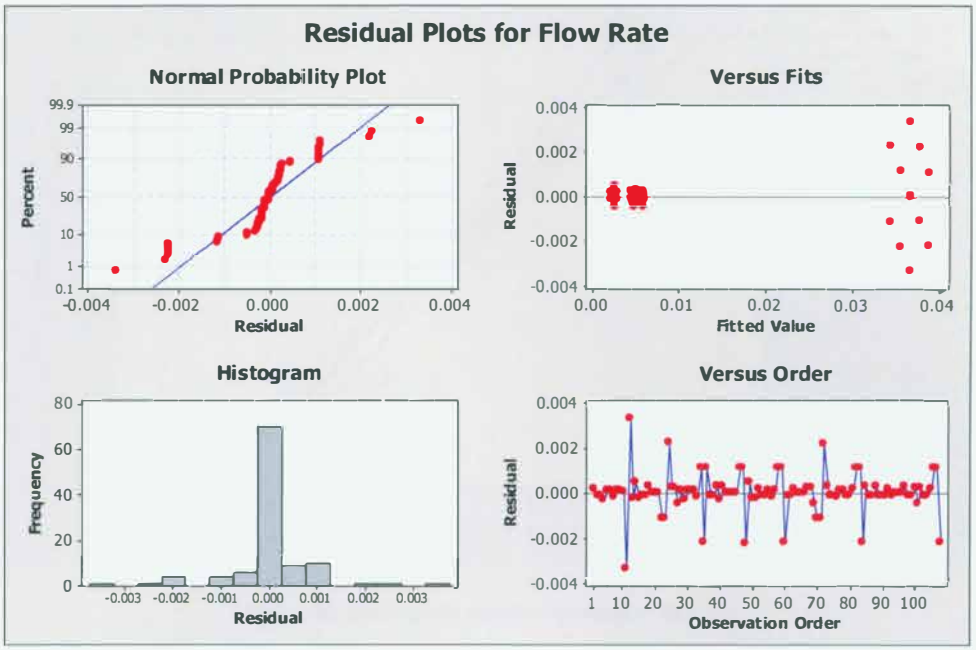

Figure 37: Residual plots for mass flow rate

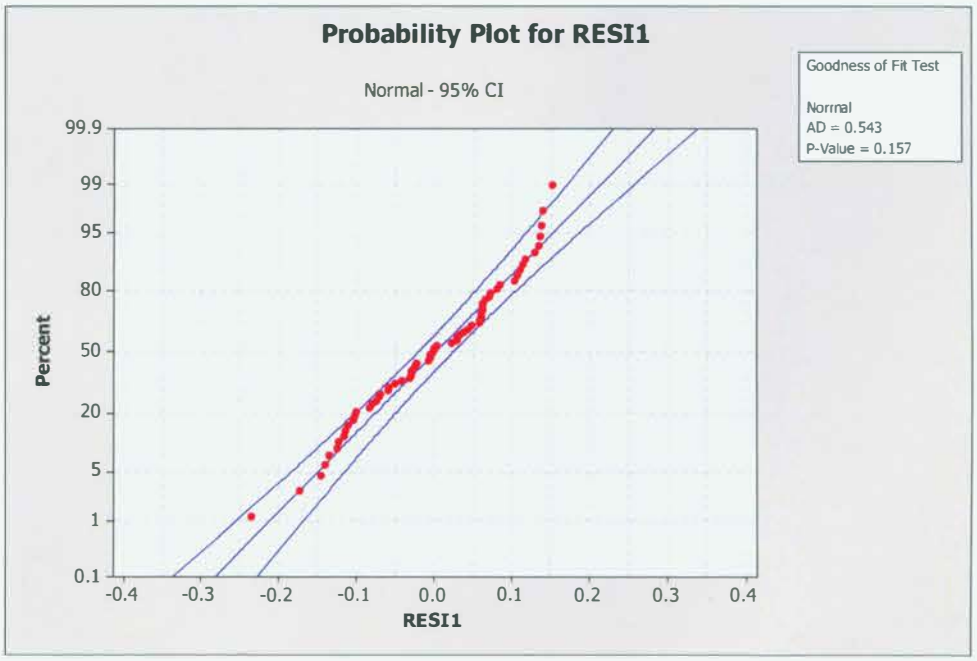

Figure 38: Probability plot for residuals – yellow ink

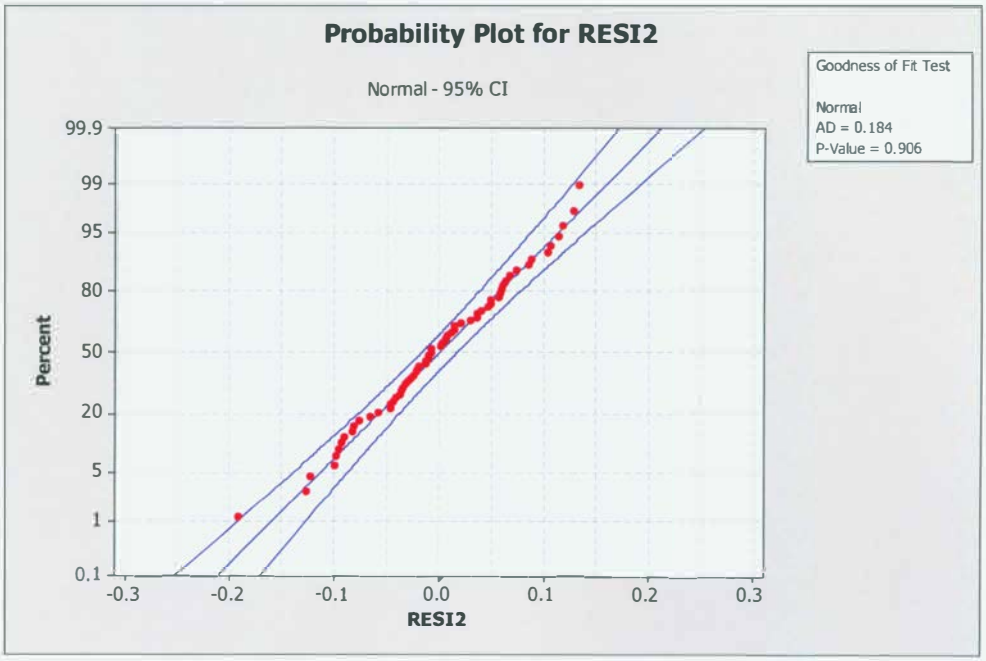

Figure 39: Probability plot for residuals – blue ink